

pubs.acs.org/Macromolecules Article

Crazing and Toughness in Diblock Copolymer-Modified Semicrystalline Poly(L-lactide)

Charles J. McCutcheon, Boran Zhao, Christopher J. Ellison,* and Frank S. Bates*



Cite This: Macromolecules 2021, 54, 11154–11169



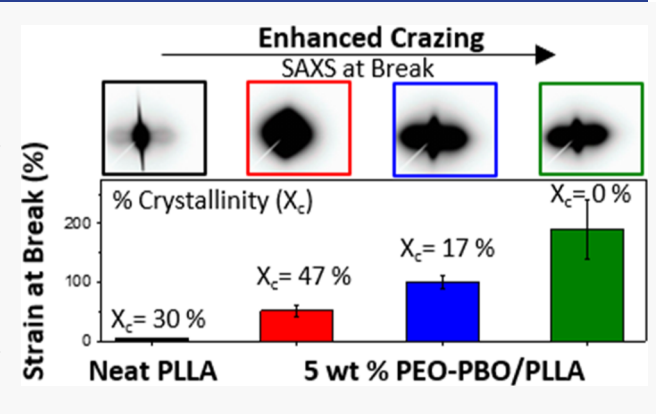
ACCESS

Metrics & More

Article Recommendations

Supporting Information

ABSTRACT: Sustainable semicrystalline poly(L-lactide) (PLLA) was melt mixed with 5 wt % poly(ethylene oxide)-b-poly(butylene oxide) (PEO-PBO) diblock copolymer, resulting in blends that display an exceptional combination of properties. The blends were annealed at various temperatures, leading to different degrees of crystallinity. The addition of 5 wt % PEO-PBO produced finely dispersed liquid particles that caused a significant reduction in the time for crystallization after quenching from the melt, where $T_{\rm m} = 166~{\rm ^{\circ}C}$. At 95 °C, the halftime for crystallization was $t_{1/2}(95~{\rm ^{\circ}C}) = t_{1/2}^{\rm o}/7$, while at 135 °C, $t_{1/2}(135~{\rm ^{\circ}C}) = t_{1/2}^{\rm o}/5$, where $t_{1/2}^{\rm o}$ is the time required to obtain 50% of the final extent of crystallization with pure PLLA. The block copolymer particles also enhanced the ductility of the blends by facilitating stress-induced cavitation and uniform crazing without impacting the modulus. Tensile toughness increased



by 7–15 fold, scaling inversely with the degree of crystallinity. The deformation mechanism was investigated by small- and wide-angle X-ray scattering as a function of applied strain, revealing that the craze volume is dependent on crystallinity, while the crystal structure displayed minimal changes. Regardless of the extent of crystallinity, crazing was found to be the primary deformation mechanism, countering the ductile-to-brittle transition associated with the aging of PLLA. Adding 5 wt % PEO-PBO extends the strain at break from 4% for pure PLLA after 2 days to more than approximately 50% after 85 or more days of aging. These findings, along with the industrially relevant blend preparation method, reveal that PEO-PBO is a unique and potent additive that could expand the applications served by PLLA, promoting a more sustainable future.

1. INTRODUCTION

Most petroleum-derived plastics do not degrade in the environment. Hence they accumulate in landfills or pollute ecosystems, 1,2 a problem exacerbated by the ubiquity of singleuse plastics. 1,3 Establishing a more sustainable future hinges on plastics that can be reused, composted, or recycled without compromising material performance. Poly(lactide) (PLA), a bio-sourced, 4,5 industrially compostable, 5-7 and commercially produced material, 8,9 with an annual global production of 190,000 tons (2019)¹⁰ is an example of such a sustainable plastic. PLA is primarily synthesized from either D,L-lactide, which produces an amorphous atactic polymer (PDLLA), or Llactide which yields the semicrystalline isotactic polymer poly(L-lactide) (PLLA). The presence of crystalline domains leads to several enhanced physical properties relative to the glassy version, including a higher upper service temperature, 11-13 increased modulus and yield stress, and improved moisture barrier properties, 14 making PLLA more attractive for various applications. Despite its sustainable nature and desirable mechanical properties, PLA, regardless of tacticity, is brittle and undergoes rapid physical aging (ca. embrittles within hours of melt processing), 15-20 which limits its utility in food packaging and the single-use plastics market in general.

A successful approach to toughen brittle amorphous and semicrystalline plastics such as PLLA $^{21-26}$ is by blending with immiscible rubbery homopolymers. The resulting rubber particles act as stress concentrators capable of initiating plastic deformation, leading to a tough plastic. A key design principle of this approach is the development of a morphology with appropriately sized particles through preassembly or application of tailored mixing techniques. Achieving specified mechanical properties, such as ductility, often requires a high mass loading (ca. > 10 wt %) of rubbery homopolymers, leading to a lower $T_{\rm g}$, reduced modulus, and lower yield stress for the blend. An alternative approach is to blend PLA with a diblock copolymer; this technique has been used to toughen PDLLA at low mass loadings (i.e., 5 wt %). $^{29-34}$ In our recent work, 34 we blended low-molecular-weight poly(ethylene

Received: August 12, 2021
Revised: November 1, 2021
Published: November 30, 2021





Table 1. Chemical Structures and Molecular Characteristics of Polymers Used in This Study

Polymer	Polymer Structure	M _n (kg/mol)	PEO Volume Fraction ^d	Dispersitye
PLLA		78ª		1.48
PEO-PBO	$($ $)_{m}$ $($ $)_{n}$	7.4 ^b	0.35	1.04
PEO	⟨ ~°} _x	5.0°	1	1.02

 $^aM_{\rm n}$ was measured by size-exclusion chromatography-multiangle light scattering (SEC-MALS) with tetrahydrofuran (THF) mobile phase and dn/dc=0.047 calculated assuming 100% sample recovery. $^bM_{\rm n}$ was measured by laser-assisted MALDI. $^cM_{\rm n}$ was measured by end group analysis using 1 H NMR. d PEO volume fraction was calculated based on 1 H NMR measurements assuming $\rho_{\rm PEO}=1.07$ g/cm 3 and $\rho_{\rm PBO}=0.92$ g/cm 3 according to ref 42. c Dispersity was measured by SEC-MALS with a THF mobile phase.

oxide)-b-poly(butylene oxide) (PEO-PBO) with PDLLA, resulting in a tough blend at concentrations as low as 1.8 wt % PEO-PBO. When subjected to an applied stress, the PEO-PBO particles cavitate and act as stress concentrators, which facilitate controlled crazing. These blends remained tough for more than 100 days following thermal processing due to an aging-independent crazing mechanism; in contrast, unmodified PLA becomes brittle in roughly 1 day. Our goal in this work is to extend this success with PDLLA to an investigation of the influence of PEO-PBO on semicrystalline PLLA.

Crystalline domains in semicrystalline polymers have been shown to impact the development of crazes, ^{35,36} alter the competition between crazing and shear yielding, ^{37,38} and disrupt stress distribution within a plastic. ^{35,37,39} Increasing crystallinity also has been reported to slow the rate of physical aging. ^{40,41} However, there are no systematic studies that focus on these physical phenomena in the presence of diblock copolymer particles.

In this work, PEO-PBO was melt blended with PLLA, yielding a uniform dispersion of liquid particles. The impact of the PEO-PBO particles on the kinetics of nucleation and growth of crystallinity and on the overall extent of crystallization of PLLA was investigated using differential scanning calorimetry (DSC) experiments. Tensile testing was employed to evaluate the effectiveness of PEO-PBO particles in toughening and alleviating aging of the semicrystalline plastic. Small-angle X-ray scattering (SAXS) and wide-angle X-ray scattering (WAXS) measurements revealed how the combined effects of crystalline domains and PEO-PBO particles alter the deformation mechanism of the blends.

2. EXPERIMENTAL SECTION

2.1. Materials. Semicrystalline PLLA (PLA4032D) was purchased from NatureWorks. Diblock copolymer (PEO-PBO) was purchased from Olin Corporation under the trade name FORTEGRA 100. This diblock copolymer is a disordered liquid at room temperature. PEO homopolymer was purchased from Sigma-Aldrich. The chemical structures and molecular characteristics of the PLLA, PEO, and PEO-PBO are provided in Table 1.

2.2. Sample Preparation. *2.2.1. Neat PLLA.* PLLA pellets were processed using a 16 mm twin screw extruder (Thermo Electron PRISM, L/D = 24:1) operating at 60 rpm and at temperatures of 140, 160, 180, and 200 °C from hopper to die. Extruded PLLA was cooled in a water bath then machine pelletized. The extruded pellets were then reprocessed in the twin screw extruder using the same conditions

as the first processing step to mimic the masterbatch-dilution method for preparing PEO-PBO/PLLA blends. All pellets were vacuum-dried at 45 $^{\circ}$ C for 24 h before each processing step.

2.2.2. PEO-PBO/PLLA Blends. Blends containing 5 wt % PEO-PBO in PLLA were prepared using a masterbatch-dilution method described previously. A concentrated masterbatch was prepared by blending PLLA and liquid PEO-PBO with a twin screw extruder using the same parameters as those used to prepare neat PLLA. To control the PEO-PBO concentration, PEO-PBO was added at a constant rate using a syringe pump. The actual concentration of the PEO-PBO in the masterbatch was determined with ¹H NMR. The masterbatch pellets were diluted by mixing with additional PLLA and then reprocessed with the twin screw extruder using the same processing conditions, resulting in a 5 wt % PEO-PBO/PLLA blend. Both PLLA, PEO-PBO, and the masterbatch were all vacuum-dried at 45 °C for 24 h before processing. The PEO-PBO concentrations in the final blends were confirmed with ¹H NMR.

2.2.3. PEO/PLLA Blends. Due to the small experimental quantities required, the PEO/PLLA blend was prepared using a microcompounder (Xplore) with a 5 mL capacity. PEO and PLLA were loaded into the hopper at 5 wt % PEO and melt blended at 180 °C and 100 rpm for 5 min. The extrudate was chilled using liquid nitrogen. The final PEO concentration was verified by ¹H NMR.

2.3. Characterization. 2.3.1. Tensile Testing. The mechanical properties of neat PLLA and PEO-PBO/PLLA and PEO/PLLA blends were determined by uniaxial tensile testing. Dried pellets were compression molded (Carver hydraulic press) at 175 °C for 3 min, followed by quenching (<1 min) to room temperature with water cooling yielding amorphous films \sim 300 μ m thick. Some samples were further processed by annealing at either 135 or 95 °C for varying times (0-3.5 min) to control the degree of crystallinity. These samples are labeled as XX/PLLA_{YY/ZZ}, where XX denotes the additive, YY indicates the annealing temperature, and ZZ specifies the annealing time (e.g., PEO-PBO/PLLA_{135/3.5} signifies a blend of PEO-PBO and PLLA annealed at 135 °C for 3.5 min). The films were cut into dumbbell-shaped tensile bars using a specimen cutter (Dumbbell Co., Ltd. SDL200, equipped with an SDMK-1000 dumbbell cutter) in accordance with ASTM D1708. Tensile bars were elongated at room temperature using a tensile tester (Instron 5966) operated at 1 mm/min crosshead speed in accordance with ASTM D1708. The tensile tests were video recorded to visualize the craze deformation process (whitening) and to monitor sample width with strain. Upon failure, the thickness of the samples was measured with calibers. Young's modulus (E), yield stress ($\sigma_{\rm Y}$), tensile toughness, and elongation at break $(\varepsilon_{\mathrm{B}})$ were calculated from the stress-strain data, where ± represents one standard deviation about the mean. Seven replicates were completed for each sample aged for 2 days and five replicates were completed for each sample aged > 2 days.

Table 2. Summary of Thermal Properties on the First DSC Heating Scan at 10 °C/min for PLLA, PEO/PLLA Blends, and PEO-PBO/PLLA Blends Annealed at Different Temperatures

sample	anneal temp. ($^{\circ}$ C)	anneal time (min)	$T_{\rm g}$ (°C)	$T_{cc} (^{\circ}C)^a$	$\Delta H_{\rm c} \left(J/g \right)^{b}$	$T_{\rm m} ({}^{\circ}C)^{c}$	$\Delta H_{\rm m} (J/g)^d$	$X_{\rm c} \ (\%)^{e}$
PLLA	175 ^f	_	59	111	34	163	34	0
PLLA	135	3.5	60	93	9	168	38	30
PLLA	95	3.5	63	86	1	166	11	10
5 wt % PEO	175 ^f	_	45	98	28	168	28	0
5 wt % PEO	135	3.5	42	112	2	166	44	45
5 wt % PEO	95	3.5	40	118	3	168	33	32
5 wt % PEO-PBO	175 ^f	_	50	100	31	166	31	0
5 wt % PEO-PBO	135	3.5	50	_	0	166	44	47
5 wt % PEO-PBO	135	0.75	50	86	6	165	39	35
5 wt % PEO-PBO	95	3.5	50	_	0	166	34	36
5 wt % PEO-PBO	95	1.25	51	93	17	166	33	17

^aThe maximum of the exothermic peak was taken as the cold crystallization temperature. ^bEnthalpy of crystallization was determined based on the integrated area associated with the crystallization peak. ^cThe minimum of the endothermic peak was taken as the melting temperature. ^dEnthalpy of melting was determined from the integrated area associated with the melting peak. ^cCrystallinity was calculated by $(\Delta H_{\rm m} - \Delta H_{\rm c})/\Delta H_{\rm m,100} \times 100$ to measure the crystallinity that resulted from the processing conditions. Where $\Delta H_{\rm m,100}$ is the enthalpy of melting for PLA with 100% crystallinity and is equal to 93.7 J/g. ⁴⁴ fSample was compression molded at 175 °C and then quenched to room temperature quickly (<1 min), resulting in an amorphous sample.

2.3.2. Scanning Electron Microscopy and Particle Size Analysis. Samples of neat PLLA and PLLA blends were submerged in liquid nitrogen for 1 min then cryo-fractured. Fracture surfaces were washed with methanol to remove the additive, mounted on a scanning electron microscopy (SEM) stub and sputter-coated with 5 nm of iridium. The surfaces were imaged with a Hitachi S-4700 scanning electron microscope, and the images were analyzed using ImageJ to calculate an area-weighted average particle diameter following a procedure described elsewhere; ⁴³ listed uncertainties represent one standard deviation about the mean.

2.3.3. Differential Scanning Calorimetry. Thermal properties of neat PLLA and PLLA blends were determined using a Mettler Toledo DSC 1. Approximately 5 mg of the sample was loaded into an aluminum pan and hermetically sealed but with a pinhole in the lid. The glass transition temperature (T_g) , % crystallinity (X_c) , melting temperature (T_m) , and cold crystallization temperature (T_{cc}) were determined as a function of processing procedures during the first heating cycle as samples were heated from 0 to 210 °C at 10 °C/min. To study crystallization kinetics, amorphous PLLA, PEO/PLLA blends, and PEO-PBO/PLLA blends were prepared by compression molding at 175 °C for 3 min, followed by quenching (<1 min) to room temperature with water cooling. These amorphous samples were annealed in the DSC for 45 min at either 95 or 135 °C and the heat flow associated with the crystallization exotherm was integrated as a function of time and plotted as relative crystallinity versus time $(X_c \text{ at time t normalized by } X_c \text{ at t} = 45 \text{ min}) \text{ using } 93.7 \text{ J/g as the}$ enthalpy of melting for PLLA with 100% crystallinity.⁴⁴ By 45 min, the relative crystallinity achieved a stable value for all samples. All DSC experiments were performed under an inert nitrogen atmosphere.

2.3.4. Small-Angle X-Ray Scattering. Synchrotron SAXS data were acquired from the DND-CAT 5ID-D beamline at the Advanced Photon Source (APS) (Argonne, IL) with a photon wavelength of λ = 0.7293 Å. 1-D scattering patterns of (1) intensity versus azimuthal angle, from -50 to 105° (with 90° as the strain direction), which is the largest angular range attainable, were obtained by radial integration, and (2) intensity versus scattering wavevector q = $4\pi\lambda^{-1}\sin(\theta/2)$ were obtained by integration over azimuthal angles from -10 to 10° of 2-D scattering patterns. Tensile bars were first elongated after 2 days of aging at the University of Minnesota (UMN). The elongated tensile bars were then mounted and shipped to the APS and examined by SAXS 6 days after stretching (8 days after processing). All stretched tensile bars were aligned vertically in the X-ray beam. To make comparisons between samples, the scattering intensities were normalized by the sample thickness and labeled as "Intensity (normalized)".

3. RESULTS AND DISCUSSION

3.1. Morphology and Thermal Properties of the Blends. In this section, we examine the influence of PEO-PBO liquid particle inclusions on the thermal properties and crystallization kinetics of PLLA blends compared to neat PLLA. PEO when mixed with PLLA produced homogeneous miscible blends that were evaluated at the same mass loading as the diblock copolymer as a control. The $T_{\rm g}$ values of all blends are listed in Table 2. A decrease in $T_{\rm g}$ for PLLAcontaining PEO is consistent with the miscibility of PEO in PLA, and partial miscibility of PEO-PBO in this plastic. Amorphous samples of PLLA, PEO/PLLA, and PEO-PBO/ PLLA were annealed at either 95 or 135 °C for 45 min in the DSC to analyze crystallization kinetics. These two isothermal annealing temperatures were selected because 135 °C is close to the temperature associated with maximum spherulite growth rate, while 95 °C is close to the temperature of the maximum nucleation rate.45-47

Figure 1A,B displays the relative crystallinity versus time obtained at 95 and 135 °C, respectively. Half time for crystallization $(t_{1/2})$ results are summarized in Figure 1C, where $t_{1/2}$ represents the time it takes to achieve half of the final degree of crystallization as $t \rightarrow 45$ min. PLLA is known to exhibit slow crystallization kinetics, which leads to greater processing times and costs. 48,49 The addition of 5 wt % PEO-PBO dramatically reduces $t_{1/2}$ from 550 to 77 s at 95 °C and from 175 to 37 s at 135 °C, that is, crystallization occurs 7 and 4.5 times faster, respectively, compared to neat PLLA. Faster crystallization for the PEO-PBO/PLLA blend may be attributed in part to a plasticization effect, 50,51 evidenced by a lower T_{σ} than for neat PLLA. Plasticizers are expected to increase chain mobility, making it easier for chains to rearrange into crystalline lamellae. However, PEO-PBO/PLLA displays smaller $t_{1/2}$ values than PEO/PLLA at both annealing temperatures (Figure 1A-C) despite the later exhibiting a lower T_g leading us to conclude that plasticization is not the sole effect. An additional factor arises from the phase-separated PEO-PBO particles, which can act as heterogeneous nucleation sites; 52-54 no such sites exist in the miscible PEO/PLLA blend. Uniformly dispersed PEO-PBO particles \sim 0.95 μ m in diameter are evident in the PEO-PBO/PLLA blends, as illustrated in

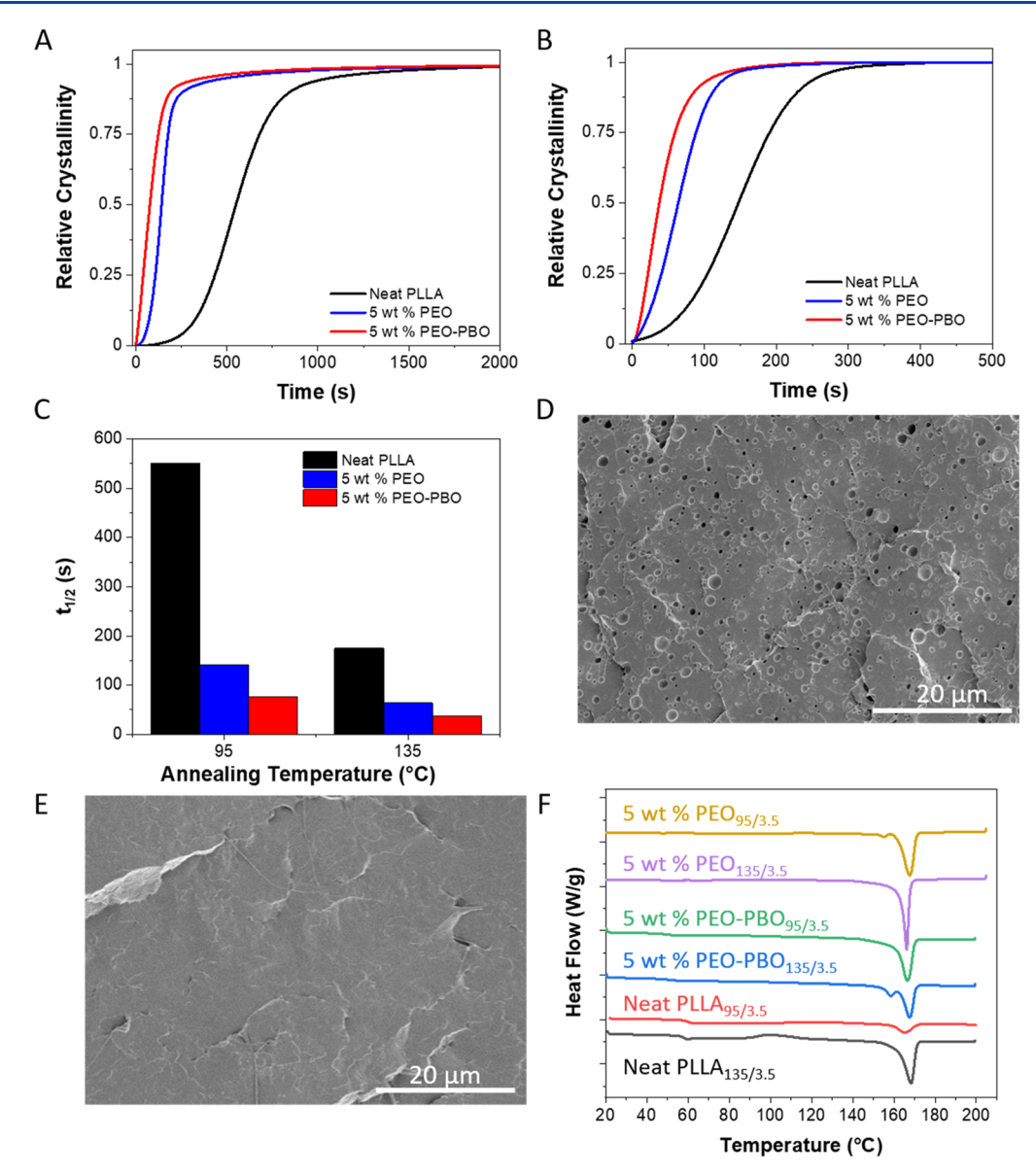


Figure 1. Crystallization kinetics of neat PLLA, 5 wt % PEO/PLLA, and 5 wt % PEO-PBO/PLLA annealed at 95 °C (A) and 135 °C (B). (C) Summary of $t_{1/2}$ results for different annealing temperatures. SEM images of (D) 5 wt % PEO-PBO/PLLA and (E) 5 wt % PEO/PLLA blends after compression molding, cryo-fracturing, and rinsing with methanol. (F) DSC thermograms (exo up) of neat PLLA and various PLLA blends annealed at different temperatures. The data are shifted vertically for clarity.

Figure 1D, versus a featureless morphology in the PEO/PLLA blends shown in Figure 1E. We conclude that the presence of PEO-PBO increases the rate of PLLA crystallization through a combination of plasticization and enhanced nucleation.

Amorphous samples (rapidly quenched from 175 °C) were annealed at either 95 or 135 °C for different periods of time, yielding specimens with varying $X_{\rm c}$. For example, blends with $X_{\rm c}=35\%$ were obtained by annealing at 135 °C for 0.75 min or 95 °C for 3.5 min. A blend with $X_{\rm c}=17\%$ was produced by annealing at 95 °C for 1.25 min. Figure 1F displays representative DSC scans (first heating at 10 °C/min) obtained from neat PLLA, 5 wt % PEO/PLLA, and 5 wt % PEO-PBO/PLLA, each annealed for 3.5 min at 135 and 95 °C. We focus on the first heating results to study the effect of sample preparation on the mechanical and thermal properties. Both blends and neat PLLA samples exhibit the same peak melting temperature $T_{\rm m}\cong 166$ °C but varying $X_{\rm c}$ and $T_{\rm g}$ and variable presence of a cold crystallization peak at $T_{\rm cc}$ (cold

crystallization temperature); data for all the samples evaluated by DSC are listed in Table 2. Neat PLLA and PEO/PLLA samples annealed for 3.5 min, and some PEO-PBO/PLLA samples annealed for < 3.5 min, exhibit an exothermic crystallization peak at T_{cc} (see Supporting Information, Figure S1 for additional DSC thermograms). This indicates that the samples did not completely crystallize during the annealing period. The PEO-PBO particle size was independent of annealing conditions and for each blend the diameter was \sim 0.95 μ m with a small standard deviation of 0.1 μ m [see the Supporting Information for additional SEM images (Figure S2) and Table S1 summarizing the particle diameter measurements]. The PEO-PBO particle dispersion in PLLA is depicted in Figure 2. We describe these particles as "selfcompatibilized", with PEO blocks (blue) presumed to be localized at the particle interface due to favorable mixing with PLA, 55,56 while the particle interior consists of disordered PEO-PBO chains (purple). Images of the particle and

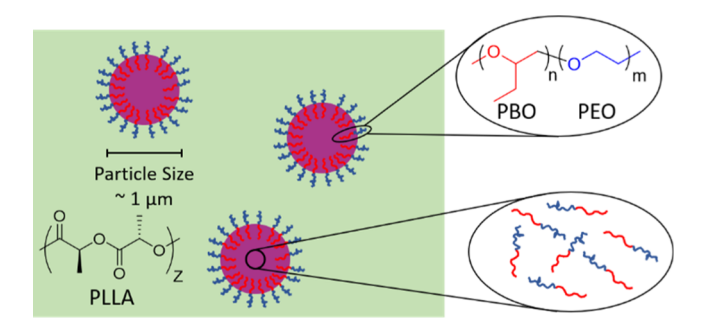


Figure 2. PEO-PBO particles dispersed in a PLLA matrix (green), where we posit that the PEO blocks are preferentially located at the particle/matrix interface, and the particle interior comprises disordered PEO-PBO chains. The size of the PEO-PBO chains is enhanced relative to the particle size for presentation purposes.

crystalline morphologies obtained by atomic force microscopy are provided in the Supporting Information (Figure S3).

3.2. Semicrystalline Morphology. The DSC results provide for a macroscopic assessment of crystallinity and crystallization kinetics as a function of the thermal processing history. However, based on previous results, 39,57 the crystalline morphology also significantly impacts the mechanical properties of the blends. Therefore, SAXS measurements were conducted to better understand the initial crystalline morphology of the blend. The long period (L_p) of the lamellae was obtained from Bragg's law, $L_p = 2\pi/q_{\rm max}$, where $q_{\rm max}$ is the position of the principal peak in the 1-D SAXS pattern. Azimuthally integrated 1-D I versus q plots obtained from undeformed (0% strain) specimens are shown in Supporting Information Figure S4, and the L_p values are listed in Table 3.

Table 3. L_p , L_a , and L_c of Neat PLLA and PEO-PBO/PLLA Blends Annealed at Various Conditions

sample	anneal temp. (°C)	anneal time (min)	X_{c} (%)	$\binom{L_{\mathrm{p}}}{(\mathrm{nm})}$	$\binom{L_{\rm c}}{({ m nm})}$	$L_{\rm a} m (nm)$
PLLA	175 ^a	_	0	_	_	-
PLLA	135	3.5	30	24.3	7.1	17.2
PLLA	95	3.5	10	_	-	-
5 wt % PEO-PBO	175 ^a	-	0	_	-	-
5 wt % PEO-PBO	135	3.5	47	26.7	12.3	14.9
5 wt % PEO-PBO	135	0.75	35	25.7	8.8	16.9
5 wt % PEO-PBO	95	3.5	36	18.6	6.4	12.2
5 wt % PEO-PBO	95	1.25	17	-	-	-

"Sample was compression molded at 175 °C and then quenched quickly (<1 min), resulting in an amorphous sample.

The crystalline lamella thickness $(L_{\rm c})$ can be calculated from the relation

$$L_{\rm c} = X_{\rm c} \left(\frac{\rho}{\rho_{\rm c}}\right) L_{\rm p} \tag{1}$$

where ρ is the density of the sample and $\rho_{\rm c}=1.29~{\rm g/cm^3}$ is the density of crystalline PLLA. The samples annealed at 135 °C displayed larger values of $L_{\rm p}$ and lamellar thicknesses, regardless of $X_{\rm c}$. At the faster crystallization rate, $L_{\rm c}$ and thus $L_{\rm p}$ both increase. The amorphous lamella thickness ($L_{\rm a}$) can be

calculated as $L_{\rm a}=L_{\rm p}-L_{\rm c}$. $L_{\rm a}$ is closely related to the probability that a tie chain will be present in the amorphous region. The concentration of tie chains impacts the transfer of stress from the amorphous regions to the stiffer crystalline regions. ⁵⁹⁻⁶¹ Note that the low crystallinity in PEO-PBO/PLLA_{95/1.25} is manifested by the absence of a peak in the SAXS pattern (Supporting Information, Figure S4).

3.3. Mechanical Properties. Tensile tests were performed at a strain rate of 1 mm/min at room temperature on neat PLLA, PEO/PLLA, and PEO-PBO/PLLA blends after 2 days of aging. The amorphous samples were molded at 175 °C and then rapidly quenched (<1 min to room temperature), while the semicrystalline samples were molded at 175 °C, quenched to room temperature and then annealed at either 135 or 95 °C. Representative stress-strain data are displayed in Figure 3A and a summary of the mechanical properties are presented in Table 4. For the neat (pure) PLLA, the yield stress, σ_{Y} , is relatively insensitive to X_c , indicative of a yielding process that involves both the glassy and crystalline domains, possibly through screw dislocation motion in the crystalline regions. 62-65 Upon yielding, these specimens all exhibit a few white streaks perpendicular to the elongation direction, attributable to localized stress-induced craze formation. In contrast to σ_{Y} , E increases from 3.0 to 3.4 GPa as X_c increases from 0 to 30% due to the greater fraction of stiffer crystalline domains, consistent with other PLA studies.⁶⁶

With the addition of 5 wt % PEO into PLLA, the overall deformation behavior and mechanical property trends with $X_{\rm c}$ are similar to those with neat PLLA, although $\sigma_{\rm Y}$ and E both decrease compared to the unmodified plastic due to the plasticization by PEO. The strain remains localized in a small area as evidenced by a few white horizontal streaks in the gauge region. The main difference between neat PLLA and the PEO/PLLA blends is the modest increase in $\varepsilon_{\rm B}$ with $X_{\rm c}$ in the blended material. As PLLA crystallizes during annealing, the PEO chains are expelled from the crystalline domains elevating the concentration in the amorphous regions, allowing the plasticized amorphous regions to elongate more readily. However, the samples are still relatively brittle with $\varepsilon_{\rm B}$ 2–3 times that of neat PLLA.

Blending PEO-PBO with PLLA significantly impacts the mechanical properties of the material, as seen in Figure 3A and summarized in Table 4. All PEO-PBO/PLLA blends exhibited $\sigma_{\rm Y}$ of about 37 MPa independent of $X_{\rm c}$. Yielding can be attributed to cavitation of the liquid PEO-PBO particles as evidenced by the uniform whitening in the entire gauge area. The cavitation stress is known to be dependent on the particle diameter, 67,68 which is constant for all the blends, explaining why $\sigma_{\rm v}$ remains the same for all PEO-PBO/PLLA blends (at constant PEO-PBO loading). $^{69-71}$ The dependence of E on X_c is similar to the PEO/PLLA blends and only decreases by ~10% at each processing condition compared to neat PLLA. All the PEO-PBO/PLLA blends were ductile with $\varepsilon_{\rm B} > 50\%$ strain, a 10-fold increase compared to neat PLLA. However, ε_{B} varies between 50 and 190% strain depending on X_c which is shown graphically in Figure 3B.

As the samples are stretched, the gauge area whitens and elongation is accompanied by volume expansion reflected in a constant width and thickness (ca. within 90% of the initial value, before straining), consistent with uniform cavitation-induced crazing. All PEO-PBO/PLLA blends deformed this way up to about 50% strain. At higher strains, differences arise based on X_c as manifested in the visual appearance of the gauge

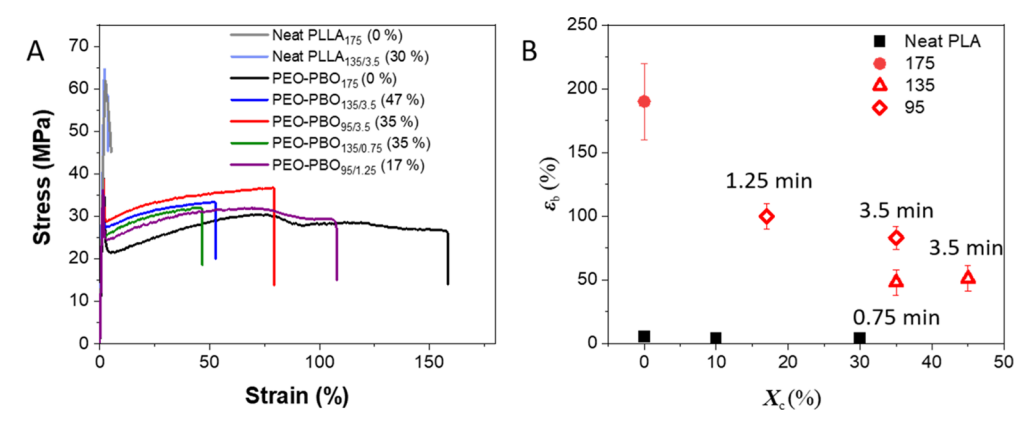


Figure 3. (A) Representative stress—strain data from neat PLLA and PEO-PBO/PLLA blends processed under different conditions producing a range of X_c values shown in parentheses. (B) ε_B versus X_c of neat PLLA (black squares) and 5 wt % PEO-PBO/PLLA blends (red symbols) varying in X_c ($X_c = 0\%$ symbols are filled, $X_c > 0\%$ symbols are open) and annealing temperature (triangles annealed at 135 °C, diamonds annealed at 95 °C). The annealing time is indicated next to the symbol.

Table 4. Summary of Mechanical Properties of Neat PLLA and PEO-PBO/PLLA Blends

sample	anneal temp. ($^{\circ}$ C)	anneal time (min)	$X_{\rm c} \ (\%)$	$\sigma_{ m Y}$ (MPa)	E (GPa)	ε_{B} (%)	toughness $\left(MJ/m^3\right)$
PLLA	175 ^a	-	0	61 ± 1	3.0 ± 0.1	5.3 ± 3	2.1 ± 1
PLLA	135	3.5	30	63 ± 1	3.4 ± 0.1	4.4 ± 1	1.7 ± 0.3
PLLA	95	3.5	10	64 ± 4	3.2 ± 0.1	3.9 ± 2	1.4 ± 0.6
5 wt % PEO	175 ^a	_	0	48 ± 2	2.7 ± 0.1	7 ± 2	3 ± 1
5 wt % PEO	135	3.5	41	48 ± 3	2.9 ± 0.1	11 ± 2	4 ± 1
5 wt % PEO	95	3.5	31	49 ± 2	2.9 ± 0.1	14 ± 3	52 ± 2
5 wt % PEO-PBO	175 ^a	_	0	38 ± 3	2.7 ± 0.1	190 ± 30	50 ± 8
5 wt % PEO-PBO	135	3.5	47	37 ± 1	3.1 ± 0.1	51 ± 10	15 ± 4
5 wt % PEO-PBO	135	0.75	35	36 ± 2	3.0 ± 0.1	48 ± 10	15 ± 6
5 wt % PEO-PBO	95	3.5	35	36 ± 1	3.0 ± 0.1	83 ± 9	28 ± 3
5 wt % PEO-PBO	95	1.25	17	36 ± 1	2.9 ± 0.1	100 ± 10	30 ± 4

[&]quot;Sample was compression molded at 175 °C and then quenched quickly (<1 min), resulting in an amorphous sample. ± indicates standard deviations.

area (see Supporting Information, Figures S6 and S7). Samples with high X_c [PEO-PBO/PLLA_{135/3.5} (X_c = 47%), PEO-PBO/PLLA_{135/1.25} (X_c = 35%), and PEO-PBO/PLLA_{95/3.5} (X_c = 35%)] continually deformed by volume expansion until failure at 50–80% strain. However, blends with low X_c [PEO-PBO/PLLA₁₇₅ (X_c = 0%) and PEO-PBO/PLLA_{95/1.25} (X_c = 17%)] continue to deform by volume expansion until undergoing a necking transition at about 75% strain, indicated by a hump in the stress—strain data, followed by elongation to higher strains. Necking indicates a change in the deformation mechanism from crazing to shear yielding.³⁴ These results suggest that the crystalline domains inhibit craze growth and necking, controlling the ductility of the blend.

Interestingly, blends annealed at 135 °C for 0.75 min (PEO-PBO/PLLA_{135/0.75}) and 95 °C for 3.5 min (PEO-PBO/PLLA_{95/3.5}) exhibit the same $X_{\rm c}=35\%$ but significantly different $\varepsilon_{\rm B}$ values. Although both blends showed significant toughness compared to neat PLLA, the blend annealed at 95 °C failed at 83 \pm 9% strain, while the blend annealed at 135 °C failed at 48 \pm 10% strain. This variation in ductility may arise from the different annealing temperatures, which affect $L_{\rm p}$ and spherulite size, that is, samples annealed at 135 °C display larger spherulites (see Supporting Information, Figure S8) and $L_{\rm p}$ values (see Table 3) than samples annealed at 95 °C. Larger spherulites have a greater propensity for catastrophic failure. The Also, a large $L_{\rm p}$ decreases the number of tie chains which

connect the amorphous and crystalline regions, leading to a reduction in mechanical properties. 61,74

3.4. Toughening Mechanism: SAXS. Analysis of SAXS measurements provides insights into craze development as the material is elongated. Ex situ SAXS measurements were carried out on stretched samples. All specimens examined were elongated after 2 days of aging following the same mechanical property testing procedure outlined earlier and then measured at Argonne National Laboratory 8 days later.

Figure 4A displays a stress-strain curve for PLLA_{135/3.5}, and Figure 4B-F illustrates corresponding 2-D SAXS patterns obtained at specified strains. For quantitative comparison, the integrated intensity $I = \int I(q) dq$ was calculated as a function of the azimuthal angle ϕ (from -50 to 105°) where $\phi = 90^{\circ}$ corresponds to the meridional axis, parallel to the applied strain, and $\phi = 0^{\circ}$ is the equatorial axis, which is perpendicular to the strain direction. *I* versus ϕ is plotted in Figure 4G. When pure PLLA is elongated to 2.0% strain, which is in the elastic regime but close to the yield point, the intensity increases slightly in the meridional and equatorial directions. This suggests initiation of relatively few isolated crazes. At the yield point (Figure 4D), the equatorial and meridional scattering intensity increases significantly (Figure 4G), indicating formation of numerous voids and crazes. The meridional scattering is consistent with void formation due to reflection from the void-bulk interfaces, 75,76 while the equatorial intensity is associated with scattering from craze fibrils

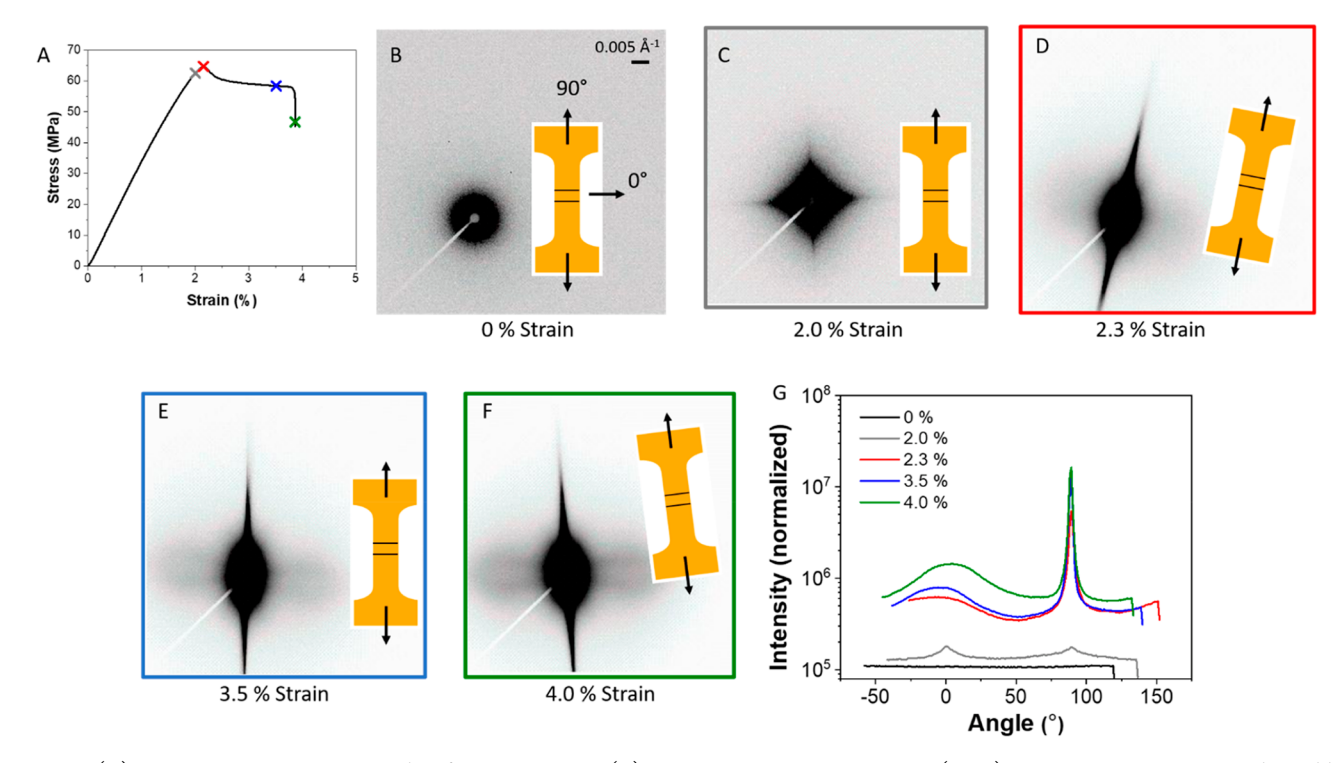


Figure 4. (A) Representative stress—strain data from PLLA $_{135/3.5}$. (B) 2-D SAXS pattern at 0% strain. (C–F) SAXS patterns at strains indicated by "X" in (A) and color-coded with outlined scattering patterns. (G) 1-D intensity versus azimuthal angle.

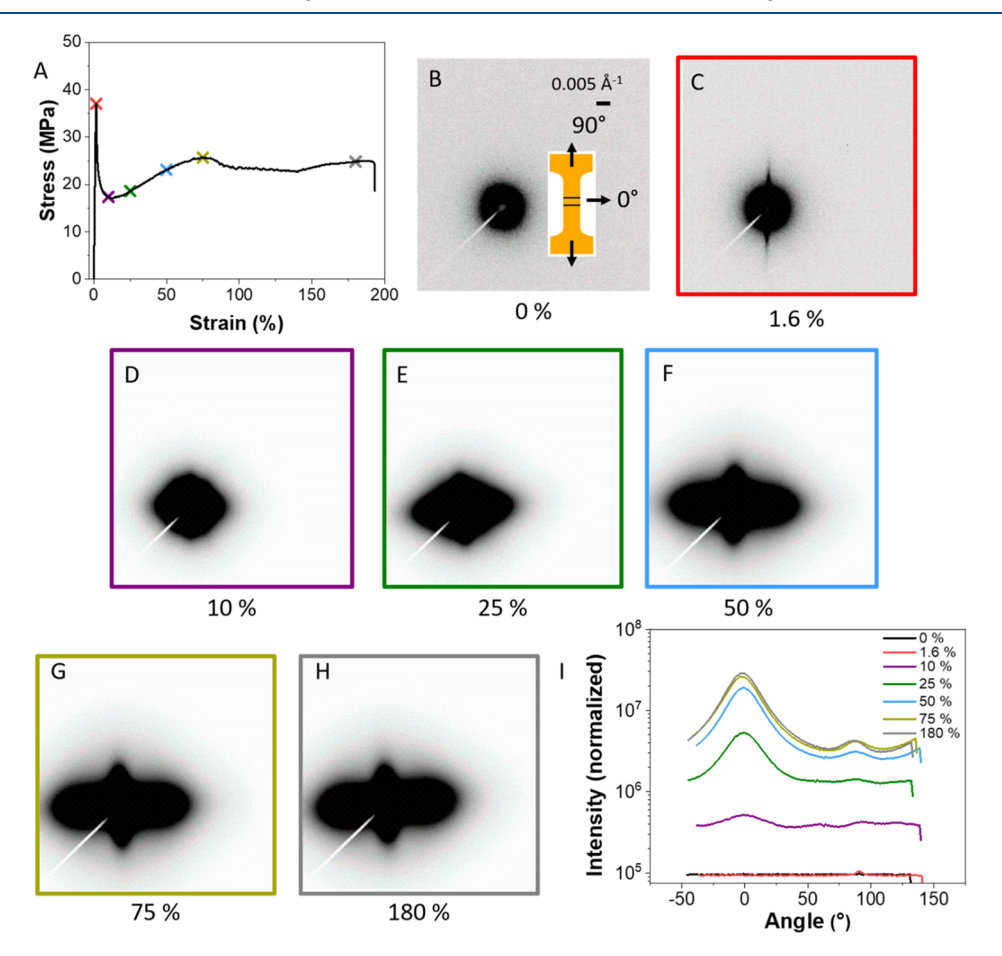


Figure 5. (A) Representative stress–strain data from PEO-PBO/PLLA₁₇₅. (B) 2-D SAXS pattern at 0% strain. (C–H) SAXS patterns at strains indicated by "X" in (A), also color-coded with outlined scattering patterns. (I) 1-D intensity vs azimuthal angle.

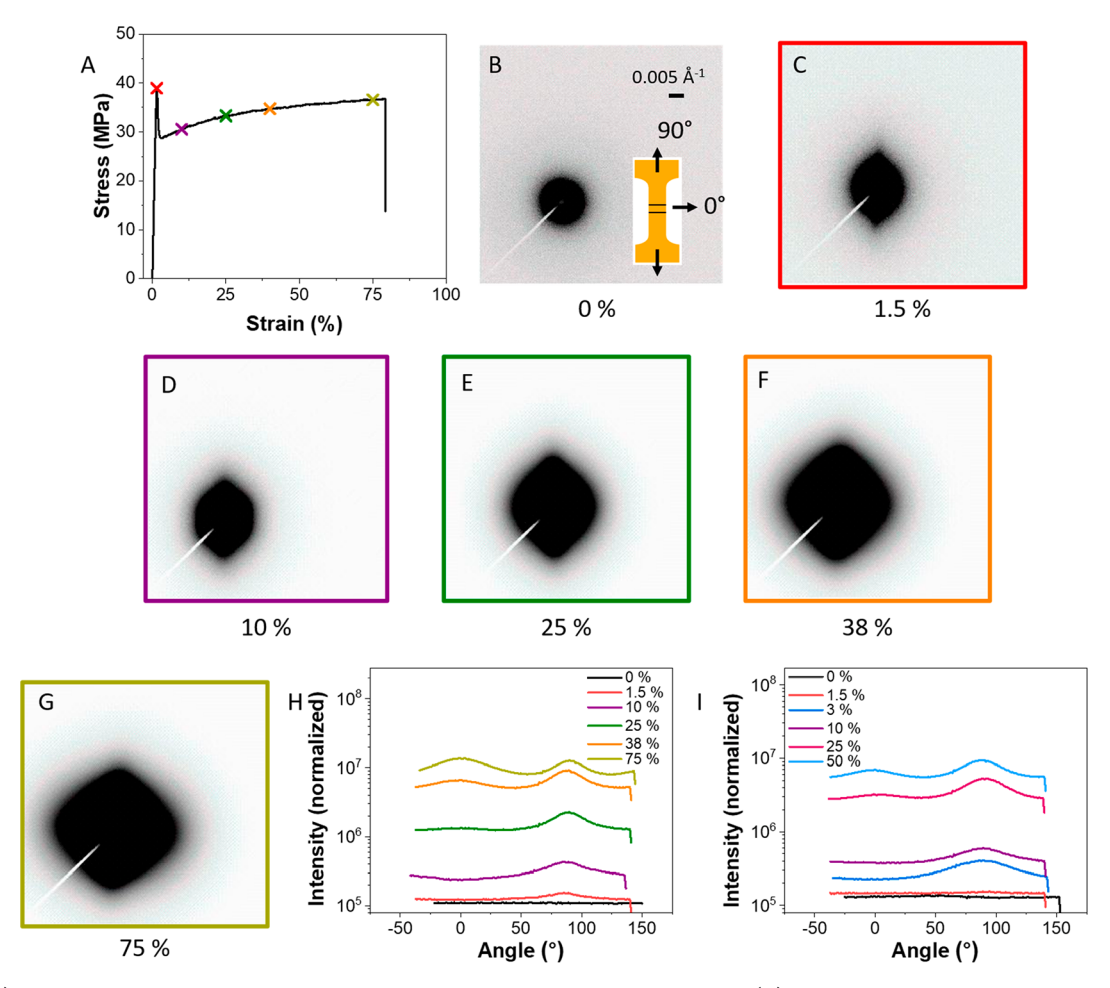


Figure 6. (A) Representative stress-strain data of high X_c blend from PEO-PBO/PLLA_{95/3.5} (B) 2-D SAXS pattern at 0 % strain. (C-G) SAXS patterns at strains indicated by "X" in (A), also color-coded with outlined scattering patterns. (H) 1-D intensity vs azimuthal angle of PEO-PBO/PLLA_{95/3.5} (I) 1-D intensity vs azimuthal angle of PEO-PBO/PLLA_{135/3.5}.

interspersed with craze voids. ^{76,77} Crazes in neat PLLA are most likely initiated by defects (e.g., dust or residual catalyst) that act as stress concentrators, ^{78,79} leading to stress buildup in a small localized area in the material. Localized deformation results in the formation of highly stressed craze fibrils surrounded by undeformed material. Following the initial jump at the yield point, the scattering intensity increases modestly between 2.5 and 4.0% strain (Figure 4G) and the sample fails at 5% strain. Prior to failure, the intensity in the meridional axis is greater than that in the equatorial axis, indicating limited craze growth.

Blending PEO-PBO with PLLA leads to a considerably tougher material with significantly different scattering results than obtained from neat PLLA. Figure 5A displays stress—strain data for PEO-PBO/PLLA₁₇₅ with $X_{\rm c}=0\%$. The accompanying 2-D SAXS patterns acquired at strains between 0% and 180% are presented in Figure 5B–H, and a plot of I versus azimuthal angle ϕ is shown in Figure 5I. These 2-D scattering patterns are similar to those reported in our previous study on noncrystalline PDLLA.³⁴ Here, crazes develop and propagate in a controlled manner with the formation of stable fibrils, which allow the sample to extend to large strains.

As the blend is elongated, there is essentially no change in the scattering pattern until the sample yields (Figure 5C) at which point a small meridional streak forms, indicative of particle cavitation. The liquid particles act as stress

concentrators, which leads to the initiation of crazes. At 10% strain (Figure 5D), there is an increase in equatorial scattering, which is associated with craze fibril scattering. 76,80,81 The scattering intensity increases continuously in the equatorial and meridional directions from 10 to 75% strain (Figure 5D-G). At strains $\geq 50\%$ (Figure 5F, 5G, 5H), the scattering pattern displays a dumbbell shape with a diffuse equatorial lobe indicative of well-developed crazes, which are continually propagating and growing (here, we note that crazes propagate perpendicular to the direction of strain leading to the formation of new fibrils, while existing fibrils elongate along the strain direction drawing new material into the widening craze). Beyond 75% strain, the scattering intensity remains nearly constant, indicating that the deformation mechanism changes from crazing to shear yielding. In contrast to neat PLLA (Figure 4), the scattering intensity along the equatorial axis is about 5-6 times greater than that recorded in the meridional axis. We interpret this as being due to a proliferation of crazes resulting from the homogeneous dispersion of liquid particles, which distributes strain localization throughout the material and facilitates uniform deformation of the gauge section of the tensile specimen.

Crystallinity resulted in significant changes in the mechanical performance of the blended specimens as discussed in the mechanical property section. Microscopically, differences in the deformation mechanism are also evident in the SAXS

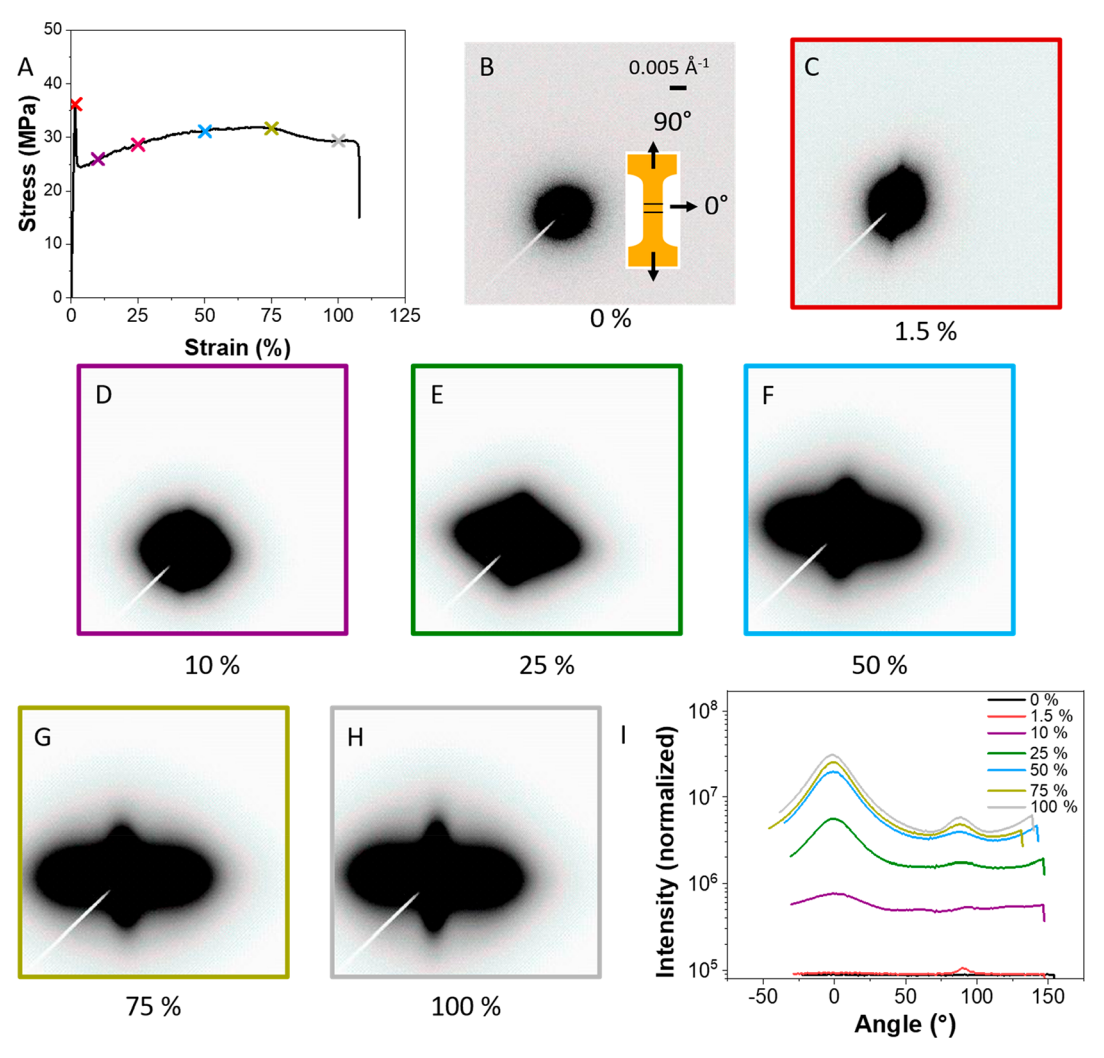


Figure 7. (A) Representative stress-strain data from PEO-PBO/PLLA_{95/1.25} (B) 2-D SAXS pattern at 0% strain. (C-H) SAXS patterns at strains indicated by "X" in (A), also color-coded with outlined scattering patterns. (I) 1-D intensity vs azimuthal angle.

experiments. To mirror the previous discussion, blends are grouped as: high X_c ($X_c \ge 35\%$) and low X_c ($X_c = 17\%$). Mechanical property and SAXS results obtained from PEO-PBO/PLLA_{95/3.5}, shown in Figure 6, are representative of all the high X_c blends. Comparisons of the 2-D SAXS patterns from PEO-PBO/PLLA₁₇₅ and the high X_c blends reveal several differences. First, for PEO-PBO/PLLA_{135/3.5} and PEO-PBO/ PLLA_{135/0.75} (see Supporting Information, Figure S9), there is a weak, diffuse ring of intensity at 0% strain, which is attributed to scattering associated with $L_{\rm p}$ of the semicrystalline matrix. Second, the high X_c blends display a lack of definitive scattering along the equatorial axis due to crazes. At 1.5% strain (Figure 6C, at the yield point), there is an increase in meridional scattering indicative of particle cavitation, which is consistent with PEO-PBO/PLLA₁₇₅ (Figure 5). As the sample is elongated, the 2-D SAXS pattern increases in intensity, eventually leading to a rhombus-like shape with little distinctive scattering in the equatorial axis. This rhombus shape is similar to what is seen in PEO-PBO/PLLA₁₇₅ at small strains of 10 and 25%, which eventually develops into the classic dumbbell-like shape associated with crazes at strains \geq 50%. We believe that the rhombus-shaped pattern is primarily a result of scattering contrast between void and polymer, while the dumbbell shape is a result of scattering from fibrils aligned

parallel to the strain direction. Absence of the dumbbell shape indicates that the high X_c blends (PEO-PBO/PLLA_{95/3.5}, PEO-PBO/PLLA_{135/3.5}, and PEO-PBO/PLLA_{135/0.75}) develop fewer crazes (at the same strain) compared to PEO-PBO/PLLA₁₇₅. Quantitatively, the lower craze density is also evident in Figure 6H,I. As described earlier, much of the increase in intensity (with strain) occurs uniformly across all angles, with a noticeable peak at 90° (meridional axis). Notably, among the high X_c blends, PEO-PBO/PLLA_{95/3.5} (Figure 6H) displays greater equatorial axis intensities than PEO-PBO/PLLA blends annealed at 135 °C (PEO-PBO/PLLA_{135/0.75} and PEO-PBO/ PLLA_{135/3.5}) (Figure 6I) with a distinct peak appearing at 38% strain compared to 50% for PEO-PBO/PLLA_{135/0.75} and PEO-PBO/PLLA_{135/3,5} and 10% for PEO-PBO₁₇₅. The intensity in the equatorial axis is proportional to the craze fibril concentration. These results help explain the difference in toughness between PEO-PBO/PLLA₁₇₅, PEO-PBO/ PLLA_{95/3.5}, PEO-PBO/PLLA_{135/0.75} and PEO-PBO/ PLLA_{135/3,5} and further indicate that the crystalline domains lead to less craze development compared to amorphous PEO-PBO/PLLA₁₇₅.

The scattering results for the low $X_{\rm c}$ blend PEO-PBO/PLLA_{95/1.25} are displayed in Figure 7. Among the crystalline samples, the mechanical properties and SAXS results of PEO-

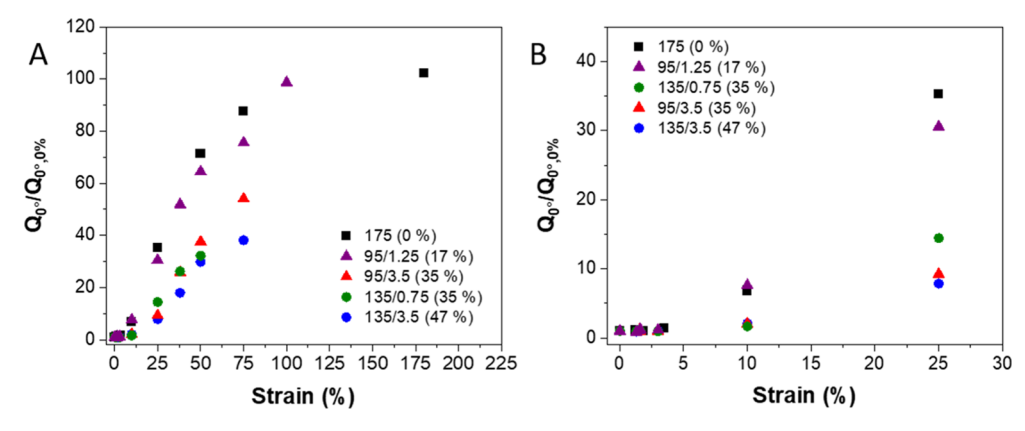


Figure 8. (A) Invariant $(Q_{0^{\circ}})$ normalized by the value at 0% strain $(Q_{0^{\circ},0\%})$ versus strain for 5 wt % PEO-PBO/PLLA for blends with varying X_c . (B) Expanded view of (A) (0-30% strain) to reveal the effects of craze formation at low strains. Samples are labeled as follows: anneal temp. (°C)/anneal time (min) with X_c in parenthesis.

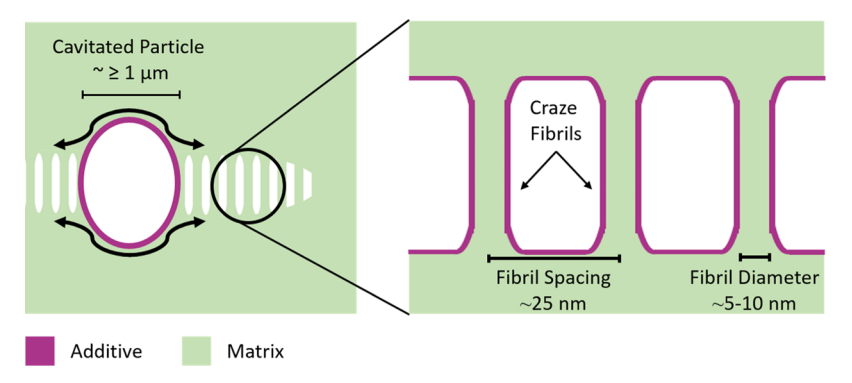


Figure 9. Additive (in purple, either PEO-PBO for this work or PB from Argon et al. ^{86–88}) draining from a cavitated particle and magnified view of additive spreading onto craze fibrils. Note that in refs 86–88, the PB particles are too small to cavitate and can only drain once a craze intersects them, while in our current study with PEO-PBO and PLLA, we believe the particles first cavitate and then drain into the associated craze.

PBO/PLLA_{95/1,25} most closely resembles those from PEO-PBO/PLLA₁₇₅. At 0% strain (Figure 7B), there is no scattering ring associated with L_p due to low crystallinity. The liquid particles cavitate at the yield point as signified by the meridional streak (Figure 7C), which is consistent with the previous blend results. As the material is elongated further, the intensity increases in both the equatorial and meridional axes, similar to the behavior of PEO-PBO/PLLA₁₇₅. The 2-D SAXS patterns display the rhombus pattern described earlier at 25% strain (Figure 7E), which eventually evolves into the diffuse dumbbell pattern by 50% strain (Figure 7F), as also seen with PEO-PBO/PLLA₁₇₅. With fewer crystalline domains, a higher concentration of crazes can propagate. The intensity in the equatorial axis (Figure 7I) is much greater than that observed in the meridional axis and the craze concentration is significantly higher than with the other semicrystalline samples. This allows the PEO-PBO/PLLA95/1.25 blend to extend to larger strains and pass through the necking transition.

To correlate the effects of X_c with crazing in the PEO-PBO/PLLA blends, 1-D I versus q SAXS plots at varying strains (Figure S10) were prepared by the integration of 2-D SAXS patterns about the azimuthal angles -10 to 10° . The increase in scattering intensity with decreasing q found in Figure S4, and for the 0% strained specimen in Figure S10, is related to instrumental effects that are generally associated with SAXS patterns obtained at a synchrotron beamline. As described below, we have determined the scattering invariant associated with crazing by restricting the integration of intensity as a

function of q to azimuthal angles of -10 to 10° . As is evident in Figure S10, the resulting I(q) traces increase in intensity by more than an order of magnitude relative to the undeformed material when sample PEO-PBO/PLLA₁₇₅ is strained by 10–50%, thus isolating the effects of particle cavitation and crazing from the instrumental background scattering. 1-D I versus q SAXS plots were used to calculate the invariant $Q_{0^{\circ}}$ which is related to the volume of crazes V according to V

$$Q_{0^{\circ}} = \int_{0}^{\infty} I(q) \times q^{2} \times dq$$
 (2)

$$Q_{0^{\circ}} = V \nu_{\rm f} (1 - \nu_{\rm f}) \Delta \rho^2 \tag{3}$$

where $\nu_{\rm f}$ is the fibril volume fraction in a craze and $\Delta\rho$ is the electron density difference between polymer and void space. Because $\nu_{\rm f}$ (at the same PEO-PBO content)⁸² and $\Delta\rho$ are constant for the blends, the changes in Q_0° are a direct result of differences in $V.^{81,82}$ $Q_0^{\circ}/Q_0^{\circ},0\%$ is plotted versus strain in Figure 8, where normalization by $Q_{0^{\circ},0\%}$ (see the Supporting Information and Figure S11 for an alternative normalization method), the invariant at 0% strain, isolates craze development in each blend independent of crystalline lamellae scattering, which varies between samples. Figure 8A covers the full range of strain values, and Figure 8B highlights the differences in Q_0° at low strain. Figure 8 demonstrates a clear relation between $X_{\rm c}$ and V. Notably, at the same $X_{\rm c}$, PEO-PBO/PLLA_{135/0.75} and PEO-PBO/PLLA_{95/3.5} display different values of Q_0° , which we attribute to differences in L_p , as explained earlier. Overall, as $X_{\rm c}$

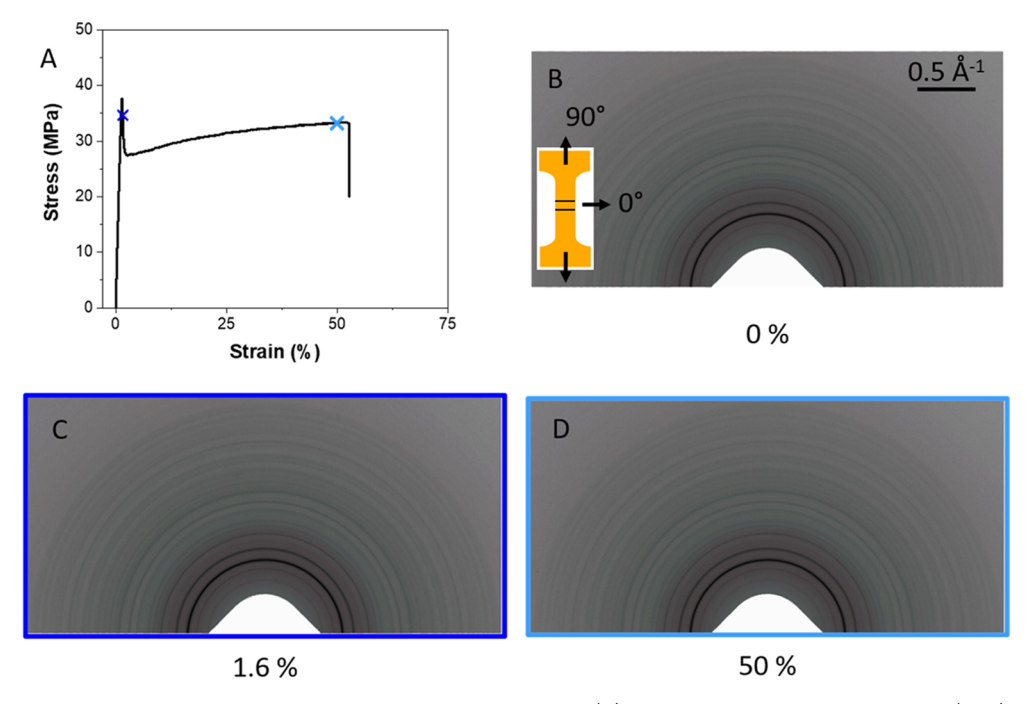


Figure 10. (A) Representative stress—strain data from PEO-PBO/PLLA_{135/3.5}. (B) 2-D WAXS pattern at 0% strain. (C,D) WAXS patterns at strains indicated by "X" in (A), also color coded with outlined scattering patterns.

increases, Q_{0° decreases. This becomes apparent starting at 10% strain and is magnified at 25% strain. At larger V, associated with the low/no $X_{\rm c}$ samples, stress is distributed throughout many craze fibrils, while at lower V the stress is concentrated within fewer craze fibrils, increasing the likelihood of craze fibril failure. This limits the ductility of the high $X_{\rm c}$ blends. Due to the constant PEO-PBO loading, the number of particles initiating crazes should be the same for all samples. Therefore, the differences in V are presumed to be due to craze propagation.

Although the craze volume differs, the void volume is likely the same between samples at the same strain due to elongation of the tensile specimens at relatively constant width and thickness. As displayed in Figures 5, 6, 7, the high X_c blends $(X_c \geq 35\%)$ exhibit larger intensity values at 90° and lower intensity values at 0° compared to the low X_c blends $(X_c \leq 17\%)$. This indicates that there is more crazing in the low X_c blends and more void formation (from other processes) in the high X_c blends. These additional voids observed in the high X_c blends can be a result of cavities forming between lamellae, or at inter spherulite boundaries X_c or can be a result of crack formation. Such voiding would account for volume expansion but would not produce load-bearing fibrils consistent with the observed reduced toughness.

The variation in ductility of the semicrystalline blends may also reflect the influence of PEO-PBO on the crazes. In related experiments, where brittle glassy polystyrene (PS, $M_{\rm w}=2.7\times10^2~{\rm kg/mol}$) was toughened by a phase separated, low molecular weight, liquid poly(butadiene) (PB, $M_{\rm w}=2.8~{\rm kg/mol}$) additive, Argon et al. $^{86-88}$ proposed a spreading mechanism depicted in Figure 9. During deformation, the additive (PB in purple) drains from the phase-separated wells and spreads onto the craze surfaces (PS in green) and sorbs into the craze boundaries. This "spreading and plasticization" process leads to craze propagation at lower stresses, resulting in greater material deformation and an overall tougher blend. PB diffusion plays a significant role in the local plasticization of PS

with the absorption time of the additive into the crazes being inversely proportional to the diffusion constant. ⁸⁷ Diffusion through semicrystalline materials is retarded because molecular transport primarily occurs through amorphous regions with crystalline domains serving as obstacles. ⁸⁹ This would be expected to lead to longer diffusion times through semicrystalline PLLA blends and therefore less plasticization occurs compared with amorphous samples. Consistent with this line of reasoning, amorphous blends craze at lower stresses and extend to larger strains.

In the current study, PEO-PBO is a low-molecular-weight liquid additive (purple in Figure 9) that phase separates from PLLA. To assess the feasibility of PEO-PBO spreading onto the PLLA craze surface, the spreading rate of PEO-PBO onto PLLA films was measured and compared to PB onto PS. We replicated the spreading experiment performed by Spiegelberg et al. 90 by placing a small drop of PEO-PBO onto a PLLA film and measuring the radius of the spreading droplet versus time, from which the spreading rate was obtained (see the Supporting Information and Figure S12 for detailed information about the spreading experiment). Note that Spiegelberg et al. 90 claim that the spreading rate onto crazes will be faster than that observed on films. The spreading rate of PEO-PBO onto PLLA is about 10 times faster than PB on PS. where PEO-PBO has the added advantage of a lower viscosity $(\eta_{\text{PEO-PBO}} \approx \eta_{\text{PB/2}})^{.91,92}$ Moreover, PEO-PBO is a surface active molecule on PLLA, which should further enhance spreading. These results lead us to conclude that craze plasticization by PEO-PBO represents a plausible toughening mechanism in the PEO-PBO/PLLA blends. These observations also may explain why amorphous PEO-PBO/PLLA blends are tougher and display a greater V than semicrystalline PEO-PBO/PLLA blends.

3.5. Toughening Mechanism: WAXS. SAXS measurements provide insights into the effect of strain on crazing while WAXS probes how strain impacts the crystalline domains. Deformation can induce a variety of structural changes to

polymer crystals including: crystalline slip, ^{27,93} shear/stack rotation, ^{37,94} crystalline morphology transition, ^{95–97} partial melting, ^{27,98,99} and strain-induced crystallization. ^{100,101} These morphological changes reflect how the stress is transferred from the amorphous to crystalline regions during deformation.

All the PEO-PBO/PLLA blends produced similar 2-D WAXS patterns as a function of strain and representative results from PEO-PBO/PLLA_{135/3.5} are presented in Figure 10. Figure 10A shows stress—strain data, and several corresponding WAXS patterns obtained at various strains are presented in Figure 10C,D (the WAXS patterns obtained at all strains are displayed in Supporting Information, Figure S13). Unlike the SAXS results, the WAXS patterns remain relatively unchanged as the sample is deformed, with no rearrangement or rotation of the crystalline domains nor broadening of the Bragg reflections or changes in the lattice spacings. Overall, it appears that the crystalline domains do not participate in the deformation mechanisms that control sample toughness.

1-D I versus q WAXS plots (Figure S14) were used for the analysis of the lattice spacing during deformation to provide additional information about the effect of elongation on crystalline domains. The lattice spacing was plotted as a function of strain for three crystalline planes: (010) at q = 1.05 $Å^{-1}$, (200)/(110) at $q = 1.19 \ Å^{-1}$, and (203) at $q = 1.35 \ Å^{-1}$, as displayed in Figure S15A–C. [Note that neat PLLA_{135/3.5} and PEO-PBO/PLLA_{95/1.25} did not display a (010) peak and therefore were not included in the (010) analysis. The lattice dimensions remain nearly constant (with small variations within 1% of the initial values) indicating that the crystalline lattice did not undergo shear or extension. 94,102 The crystallinity decreased as a function of strain but remained within 80% of the unstretched material as monitored by WAXS (see Supporting Information, Figure S16). Overall, the crystalline lattices are either engulfed into a growing craze or remain intact without deforming. Invariant WAXS results with strain suggest that strain does not lead to commonly observed crystal deformations such as orientation, elongation, or rotation and that the primary deformation mechanism is crazing (including energy associated with craze formation: disentanglement, chain scission, and crystal destruction).

3.6. Mechanical Properties as a Function of Physical Aging. PLA is well known to undergo fast physical aging, leading to embrittlement in about 1 day at room temperature. 67,18,34,103 In order to investigate the effect of X_c on physical aging, the mechanical properties of the PEO-PBO/ PLLA blends were examined as a function of aging time. Representative stress-strain results obtained from specimens of PEO-PBO/PLLA_{95/3.5} aged for up to 85 days at room temperature are presented in Figure 11; Table 5 lists the mechanical properties recorded for a range of aging times for all samples investigated in this study. Remarkably, all the diblock copolymer-modified blends exhibit sustained and relatively constant toughness for 85 to 154 days of aging. These results are in sharp contrast with the behavior of the neat PLLA with 30% crystallinity, which becomes brittle ($\varepsilon_{\rm B} \approx$ 4%) after 2 days of aging at room temperature. Regardless of the aging time, the blends undergo uniform whitening at the yield point, followed by volume expansion, elongating at relatively constant width and thickness due to the formation of voids associated with craze formation (see Figure S17). This is consistent with our previous study of PEO-PBO/PDLLA which showed that craze initiation and propagation are independent of aging time.³⁴ There is a modest dependence

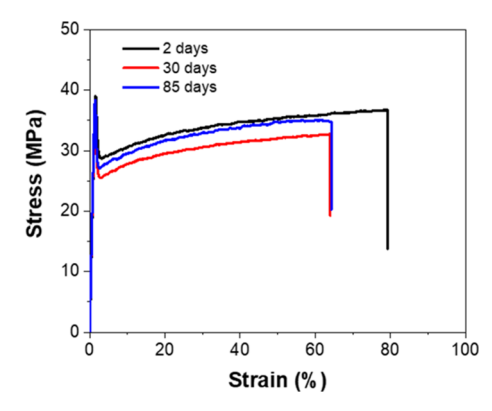


Figure 11. Representative stress-strain data from PEO-PBO/PLLA_{95/3.5} at various aging times.

of the toughness on the percent crystallinity: 44% average $\varepsilon_{\rm B}$ for specimens with 47% crystallinity (PEO-PBO/PLLA_{135/3.5}), 61% for specimens with 35% crystallinity (PEO-PBO/PLLA_{95/3.5}), and 85% for blends with 17% crystallinity (PEO-PBO/PLLA_{95/1.25}). We believe that the persistence of mechanical toughness after long aging time can be attributed to crazing as the primary deformation mechanism. $^{34,104-106}$

While all blends remain tough during aging, there is a noteworthy change in the PEO-PBO/PLLA $_{95/1.25}$ blend due to densification during aging. PEO-PBO/PLLA_{95/1.25} is the only semicrystalline blend that passes through a necking transition where the deformation mechanism shifts from crazing to shear yielding. This transition, which occurs at about 75% strain after 2 days of aging, is absent at longer aging times as the blend fails just prior to necking; the stress-strain data as a function of time for PEO-PBO/PLLA_{95/1.25} is displayed in Figure S18. This trend, present in the blend material with the lowest value of $X_{\mathcal{O}}$ is consistent with the behavior of amorphous PEO-PBO/PDLLA blends, ³⁴ in which the strain associated with the necking transition increases as a result of chain densification. Densification makes it harder for the material to flow, and thus, the necking transition stress becomes unattainable during tensile testing. Consistent with the other semicrystalline blends, at higher aging times, PEO-PBO/PLA_{95/1.25} deforms by crazing, which is unaffected by aging, and it is this mechanism that results in persistent toughness. 34,104-106

4. CONCLUSIONS

This investigation addressed three major shortcomings that prevent the widespread application of sustainable PLLA: (1) slow crystallization kinetics; (2) rapid physical aging; and (3) brittleness. The addition of a PEO-PBO diblock copolymer at 5 wt % loading alleviates these shortcomings without affecting the modulus, making it an ideal additive for PLLA. Blending PEO-PBO into PLLA results in dispersed particles that enhance the crystallization rate of PLLA compared to neat PLLA, leading to lower processing times and potentially shorter costs. These particles also greatly enhance the ductility of PLLA, resulting in a minimum 10-fold improvement in the strain at break, $\varepsilon_{\rm B}$, due to uniform crazing initiated by cavitation of the rubbery particles during deformation. The presence of crystalline domains influences the development of crazes: as the fractional crystallinity, X_c , increased, the ductility and craze volume, V, decreased. We observed no changes to the crystal structure as a function of strain, as demonstrated by WAXS. All PEO-PBO/PLLA blends were unaffected by

Table 5. Mechanical Properties of 5 wt % PEO-PBO/PLLA Blends with Variable Crystallinity and Aging Times

anneal temp. (°C)	anneal time (min)	$X_{\rm c}$ (%)	aging (days)	$\sigma_{_{ m Y}}$ (MPa)	E (GPa)	ε_{B} (%)	toughness (MJ/m^3)
175 ^a	-	0	2	38 ± 3	2.7 ± 0.1	190 ± 30	50 ± 8
135	3.5	47	2	37 ± 1	3.1 ± 0.1	51 ± 10	15 ± 4
135	3.5	47	30	36 ± 2	3.2 ± 0.1	40 ± 5	12 ± 1
135	3.5	47	85	37 ± 2	3.2 ± 0.2	41 ± 15	12 ± 6
135	0.75	35	2	36 ± 2	3.0 ± 0.1	48 ± 10	15 ± 6
135	0.75	35	9	35 ± 2	3.0 ± 0.1	48 ± 11	15 ± 7
135	0.75	35	154	33 ± 1	3.0 ± 0.2	53 ± 6	15 ± 3
95	3.5	35	2	36 ± 1	3.0 ± 0.1	83 ± 9	28 ± 3
95	3.5	35	30	39 ± 3	2.9 ± 0.1	66 ± 6	24 ± 4
95	3.5	35	85	39 ± 1	3.2 ± 0.1	69 ± 10	22 ± 4
95	1.25	17	2	36 ± 1	2.9 ± 0.1	100 ± 10	30 ± 4
95	1.25	17	9	35 ± 2	2.9 ± 0.1	78 ± 17	22 ± 6
95	1.25	17	154	32 ± 2	3.0 ± 0.1	77 ± 16	21 ± 3

[&]quot;Sample was compression molded at 175 °C and then quenched quickly (<1 min), resulting in an amorphous specimen. ± indicates standard deviations.

physical aging and remained tough for at least 85 to 154 days at room temperature, with a modest influence of X_c on ε_B . These findings, along with the results of a previous study on amorphous PDLLA, establish PEO-PBO as a uniquely effective additive for PLA that enhances the mechanical properties at relatively low loadings, thus broadening the range of potential applications for this sustainable plastic.

ASSOCIATED CONTENT

5 Supporting Information

The Supporting Information is available free of charge at https://pubs.acs.org/doi/10.1021/acs.macromol.1c01702.

Additional PEO-PBO/PLLA blend DSC curves, polarized optical microscopy images of spherulites, SEM images of PEO-PBO/PLLA blends and associated particle diameters, 1-D SAXS intensity versus q plots, atomic force microscopy images of PLLA and PEO-PBO/PLLA blend morphologies, images of deformed tensile bars, PEO-PBO/PLLA $_{135/3.5}$ 2-D SAXS patterns and 1-D intensity versus azimuthal angle plot, 1-D WAXS intensity versus q plots, I versus q plot as a function of strain for PEO-PBO/PLLA $_{175}$, alternative normalization of Q_0 versus strain plot, spreading experiments setup and results, and relative crystallinity versus strain and representative stress—strain data for PEO-PBO/PLLA $_{95/1.25}$ at various aging times (PDF)

AUTHOR INFORMATION

Corresponding Authors

Christopher J. Ellison — Department of Chemical Engineering and Materials Science, University of Minnesota, Minneapolis, Minnesota 55455, United States; Ocid.org/0000-0002-0393-2941; Email: cellison@umn.edu

Frank S. Bates – Department of Chemical Engineering and Materials Science, University of Minnesota, Minneapolis, Minnesota 55455, United States; oorcid.org/0000-0003-3977-1278; Email: bates001@umn.edu

Authors

Charles J. McCutcheon – Department of Chemical Engineering and Materials Science, University of Minnesota, Minneapolis, Minnesota 55455, United States Boran Zhao – Department of Chemical Engineering and Materials Science, University of Minnesota, Minneapolis, Minnesota 55455, United States

Complete contact information is available at: https://pubs.acs.org/10.1021/acs.macromol.1c01702

Author Contributions

C.J.M. and B.Z. are co-first authors. The manuscript was written through contributions of all authors. All authors have given approval to the final version of the manuscript.

Notes

The authors declare no competing financial interest.

■ ACKNOWLEDGMENTS

This work was supported, in part, by the farm families of Minnesota and their corn check-off investment. SAXS experiments were conducted by Steven Weigand at the Advanced Photon Source (APS), Sector 5 (DuPont-Northwestern-Dow Collaborative Access Team, DND-CAT). DND-CAT is supported by E.I. DuPont de Nemours & Co., The Dow Chemical Company, and Northwestern University. Use of the APS, an Office of Science User Facility operated for the U.S. Department of Energy (DOE) Office of Science by Argonne National Laboratory, was supported by the U.S. DOE under contract no. DE-AC02- 06CH11357. SAXS data were collected using an instrument funded by the National Science Foundation under grant no. 0960140. Parts of this work were carried out in the Characterization Facility at the University of Minnesota, which receives partial support from the NSF through the MRSEC program (DMR-2011401). A special thanks to Xiayu Peng for AFM images.

REFERENCES

- (1) Geyer, R.; Jambeck, J. R.; Law, K. L. Production, use, and fate of all plastics ever made. *Sci. Adv.* **2017**, *3*, No. e1700782.
- (2) Jambeck, J. R.; Geyer, R.; Wilcox, C.; Siegler, T. R.; Perryman, M.; Andrady, A.; Narayan, R.; Law, K. L. Plastic waste inputs from land into the ocean. *Science* **2015**, 347, 768–771.
- (3) Lau, W. W. Y.; Shiran, Y.; Bailey, R. M.; Cook, E.; Stuchtey, M. R.; Koskella, J.; Velis, C. A.; Godfrey, L.; Boucher, J.; Murphy, M. B.; Thompson, R. C.; Jankowska, E.; Castillo Castillo, A.; Pilditch, T. D.; Dixon, B.; Koerselman, L.; Kosior, E.; Favoino, E.; Gutberlet, J.; Baulch, S.; Atreya, M. E.; Fischer, D.; He, K. K.; Petit, M. M.; Sumaila, U. R.; Neil, E.; Bernhofen, M. V.; Lawrence, K.; Palardy, J. E.

- Evaluating scenarios toward zero plastic pollution. *Science* **2020**, *369*, 1455–1461.
- (4) Vink, E. T. H.; Davies, S. Life Cycle Inventory and Impact Assessment Data for 2014 IngeoTM Polylactide Production. *Ind. Biotechnol.* **2015**, *11*, 167–180.
- (5) Miller, S. A. Sustainable Polymers: Opportunities for the Next Decade. *ACS Macro Lett.* **2013**, 2, 550–554.
- (6) Lim, L.-T.; Auras, R.; Rubino, M. Processing technologies for poly(lactic acid). *Prog. Polym. Sci.* **2008**, 33, 820–852.
- (7) Kale, G.; Kijchavengkul, T.; Auras, R.; Rubino, M.; Selke, S. E.; Singh, S. P. Compostability of Bioplastic Packaging Materials: An Overview. *Macromol. Biosci.* **2007**, *7*, 255–277.
- (8) Sardon, H.; Dove, A. P. Plastics recycling with a difference. *Science* **2018**, *360*, *380*–*381*.
- (9) Albertsson, A.-C.; Hakkarainen, M. Designed to degrade. *Science* **2017**, 358, 872–873.
- (10) Jem, K. J.; Tan, B. The development and challenges of poly (lactic acid) and poly (glycolic acid). *Adv. Ind. Eng. Polym. Res.* **2020**, 3, 60–70
- (11) Deng, L.; Xu, C.; Wang, X.; Wang, Z. Supertoughened Polylactide Binary Blend with High Heat Deflection Temperature Achieved by Thermal Annealing above the Glass Transition Temperature. ACS Sustainable Chem. Eng. 2018, 6, 480–490.
- (12) Tábi, T.; Hajba, S.; Kovács, J. G. Effect of crystalline forms (α' and α) of poly(lactic acid) on its mechanical, thermo-mechanical, heat deflection temperature and creep properties. *Eur. Polym. J.* **2016**, 82, 232–243.
- (13) Hashima, K.; Nishitsuji, S.; Inoue, T. Structure-properties of super-tough PLA alloy with excellent heat resistance. *Polymer* **2010**, 51, 3934–3939.
- (14) Ahmed, J.; Varshney, S. K. Polylactides-Chemistry, Properties and Green Packaging Technology: A Review. *Int. J. Food Prop.* **2011**, *14*, 37–58.
- (15) Struik, L. C. E. Physical aging in plastics and other glassy materials. *Polym. Eng. Sci.* **1977**, *17*, 165–173.
- (16) Arnold, J. C. The effects of physical aging on the brittle fracture behavior of polymers. *Polym. Eng. Sci.* **1995**, *35*, 165–169.
- (17) Haugan, I. N.; Lee, B.; Maher, M. J.; Zografos, A.; Schibur, H. J.; Jones, S. D.; Hillmyer, M. A.; Bates, F. S. Physical Aging of Polylactide-Based Graft Block Polymers. *Macromolecules* **2019**, 52, 8878–8894.
- (18) Pan, P.; Zhu, B.; Inoue, Y. Enthalpy Relaxation and Embrittlement of Poly(l-lactide) during Physical Aging. *Macromolecules* **2007**, *40*, 9664–9671.
- (19) Theryo, G. Deformation and Physical Aging of Rubber-Modified Polylactide Graft Copolymers; University of Minnesota, 2014.
- (20) Ren, J.; Urakawa, O.; Adachi, K. Dielectric and Viscoelastic Studies of Segmental and Normal Mode Relaxations in Undiluted Poly(d,l-lactic acid). *Macromolecules* **2003**, *36*, 210–219.
- (21) Semba, T.; Kitagawa, K.; Ishiaku, U. S.; Hamada, H. The effect of crosslinking on the mechanical properties of polylactic acid/polycaprolactone blends. *J. Appl. Polym. Sci.* **2006**, *101*, 1816–1825.
- (22) Vilay, V.; Mariatti, M.; Ahmad, Z.; Pasomsouk, K.; Todo, M. Characterization of the mechanical and thermal properties and morphological behavior of biodegradable poly(L-lactide)/poly(ε-caprolactone) and poly(L-lactide)/poly(butylene succinate-co-L-lactate) polymeric blends. *J. Appl. Polym. Sci.* **2009**, 114, 1784–1792.
- (23) Bai, H.; Xiu, H.; Gao, J.; Deng, H.; Zhang, Q.; Yang, M.; Fu, Q. Tailoring Impact Toughness of Poly(l-lactide)/Poly(ε -caprolactone) (PLLA/PCL) Blends by Controlling Crystallization of PLLA Matrix. ACS Appl. Mater. Interfaces **2012**, 4, 897–905.
- (24) Anderson, K. S.; Hillmyer, M. A. The influence of block copolymer microstructure on the toughness of compatibilized polylactide/polyethylene blends. *Polymer* **2004**, *45*, 8809–8823.
- (25) Anderson, K. S.; Lim, S. H.; Hillmyer, M. A. Toughening of polylactide by melt blending with linear low-density polyethylene. *J. Appl. Polym. Sci.* **2003**, *89*, 3757–3768.
- (26) Dai, J.; Bai, H.; Liu, Z.; Chen, L.; Zhang, Q.; Fu, Q. Stereocomplex crystallites induce simultaneous enhancement in

- impact toughness and heat resistance of injection-molded polylactide/polyurethane blends. RSC Adv. 2016, 6, 17008–17015.
- (27) Argon, A. S. The Physics of Deformation and Fracture of Polymers; Cambridge university Press: United Kingdom, 2013; pp 273–324 and pp 435–500.
- (28) Bucknall, C. B. Toughened Plastics; Springer, 1977; pp 137-241.
- (29) Pluta, M.; Piorkowska, E. Tough crystalline blends of polylactide with block copolymers of ethylene glycol and propylene glycol. *Polym. Test.* **2015**, *46*, 79–87.
- (30) Kowalczyk, M.; Pluta, M.; Piorkowska, E.; Krasnikova, N. Plasticization of polylactide with block copolymers of ethylene glycol and propylene glycol. *J. Appl. Polym. Sci.* **2012**, *125*, 4292–4301.
- (31) Jia, Z.; Tan, J.; Han, C.; Yang, Y.; Dong, L. Poly(ethylene glycol-co-propylene glycol) as a macromolecular plasticizing agent for polylactide: Thermomechanical properties and aging. *J. Appl. Polym. Sci.* **2009**, *114*, 1105–1117.
- (32) Li, T.; Zhang, J.; Schneiderman, D. K.; Francis, L. F.; Bates, F. S. Toughening Glassy Poly(lactide) with Block Copolymer Micelles. *ACS Macro Lett.* **2016**, *5*, 359–364.
- (33) Gu, L.; Nessim, E. E.; Li, T.; Macosko, C. W. Toughening poly(lactic acid) with poly(ethylene oxide)-poly(propylene oxide)-poly(ethylene oxide) triblock copolymers. *Polymer* **2018**, *156*, 261–269.
- (34) McCutcheon, C. J.; Zhao, B.; Jin, K.; Bates, F. S.; Ellison, C. J. Crazing Mechanism and Physical Aging of Poly(lactide) Toughened with Poly(ethylene oxide)-block-poly(butylene oxide) Diblock Copolymers. *Macromolecules* **2020**, *53*, 10163–10178.
- (35) Morel, D. E.; Grubb, D. T. Craze behaviour in isotactic polystyrene: 1. Craze-spherulite interaction. *Polymer* **1984**, *25*, 417–429.
- (36) Olf, H. G.; Peterlin, A. Crazing and fracture in crystalline, isotactic polypropylene and the effect of morphology, gaseous environments, and temperature. *J. Polym. Sci., Polym. Phys. Ed.* 1974, 12, 2209–2251.
- (37) Kausch, H.-H.; Gensler, R.; Grein, C.; Plummer, C. J. G.; Scaramuzzino, P. Crazing in semicrystalline thermoplastics. *J. Macromol. Sci., Part B: Phys.* **1999**, *38*, 803–815.
- (38) Bai, H.; Huang, C.; Xiu, H.; Gao, Y.; Zhang, Q.; Fu, Q. Toughening of poly(l-lactide) with poly(ε -caprolactone): Combined effects of matrix crystallization and impact modifier particle size. *Polymer* **2013**, *54*, 5257–5266.
- (39) Razavi, M.; Wang, S.-Q. Why Is Crystalline Poly(lactic acid) Brittle at Room Temperature? *Macromolecules* **2019**, *52*, 5429–5441.
- (40) Zhou, H.; Lofgren, E. A.; Jabarin, S. A. Effects of microcrystallinity and morphology on physical aging and its associated effects on tensile mechanical and environmental stress cracking properties of poly(ethylene terephthalate). *J. Appl. Polym. Sci.* **2009**, *112*, 2906–2917.
- (41) Tant, M. R.; Wilkes, G. L. Physical aging studies of semicrystalline poly(ethylene terephthalate). *J. Appl. Polym. Sci.* **1981**, 26, 2813–2825.
- (42) Wu, J.; Thio, Y. S.; Bates, F. S. Structure and properties of PBO-PEO diblock copolymer modified epoxy. *J. Polym. Sci., Part B: Polym. Phys.* **2005**, 43, 1950–1965.
- (43) Foudazi, R.; Zhao, B.; Gokun, P.; Manas-Zloczower, I.; Rowan, S. J.; Feke, D. L. The Effect of Shear on the Evolution of Morphology in High Internal Phase Emulsions Used as Templates for Structural and Functional Polymer Foams. *ACS Appl. Polym. Mater.* **2020**, 2, 1579–1586.
- (44) Garlotta, D. A Literature Review of Poly(Lactic Acid). *J. Polym. Environ.* **2001**, *9*, 63–84.
- (45) Androsch, R.; Di Lorenzo, M. L.; Schick, C. Crystal nucleation in random l/d-lactide copolymers. *Eur. Polym. J.* **2016**, *75*, 474–485.
- (46) Di Lorenzo, M. L.; Androsch, R. Influence of α' -/ α -crystal polymorphism on properties of poly(l-lactic acid). *Polym. Int.* **2019**, 68, 320–334.
- (47) Di Lorenzo, M. L.; Androsch, R., Synthesis, Structure and Properties of Poly (Lactic Acid); Springer, 2018; pp 235–272.

- (48) Schmidt, S. C.; Hillmyer, M. A. Polylactide stereocomplex crystallites as nucleating agents for isotactic polylactide. *J. Polym. Sci., Part B: Polym. Phys.* **2001**, *39*, 300–313.
- (49) Nofar, M.; Zhu, W.; Park, C. B.; Randall, J. Crystallization Kinetics of Linear and Long-Chain-Branched Polylactide. *Ind. Eng. Chem. Res.* **2011**, *50*, 13789–13798.
- (50) Li, H.; Huneault, M. A. Effect of nucleation and plasticization on the crystallization of poly(lactic acid). *Polymer* **2007**, *48*, 6855–6866
- (51) Martin, O.; Avérous, L. Poly(lactic acid): plasticization and properties of biodegradable multiphase systems. *Polymer* **2001**, *42*, 6209–6219.
- (52) Chen, Y.; Zhang, Y.; Jiang, F.; Wang, J.; Xu, Z.; Wang, Z. Significant enhancement of crystallization kinetics of polylactide in its immiscible blends through an interfacial effect from comb-like grafted side chains. *Sci. China: Chem.* **2016**, *59*, 609–618.
- (53) Liu, Q.; Zhang, H.; Zhu, M.; Dong, Z.; Wu, C.; Jiang, J.; Li, X.; Luo, F.; Gao, Y.; Deng, B.; Zhang, Y.; Xing, J.; Wang, H.; Li, X. Blends of polylactide/thermoplactic elastomer: Miscibility, physical aging and crystallization behaviors. *Fibers Polym.* **2013**, *14*, 1688–1698.
- (54) Pongtanayut, K.; Thongpin, C.; Santawitee, O. The Effect of Rubber on Morphology, Thermal Properties and Mechanical Properties of PLA/NR and PLA/ENR Blends. *Energy Procedia* **2013**, 34, 888–897.
- (55) Lai, W.-C.; Liau, W.-B.; Lin, T.-T. The effect of end groups of PEG on the crystallization behaviors of binary crystalline polymer blends PEG/PLLA. *Polymer* **2004**, *45*, 3073–3080.
- (56) Lin, J.-H.; Woo, E. M. Correlation between interactions, miscibility, and spherulite growth in crystalline/crystalline blends of poly(ethylene oxide) and polyesters. *Polymer* **2006**, *47*, 6826–6835.
- (57) Razavi, M.; Zhang, W.; Khonakdar, H. A.; Janke, A.; Li, L.; Wang, S.-Q. Inducing nano-confined crystallization in PLLA and PET by elastic melt stretching. *Soft Matter* **2021**, *17*, 1457–1462.
- (58) Fischer, E. W.; Sterzel, H. J.; Wegner, G. Investigation of the structure of solution grown crystals of lactide copolymers by means of chemical reactions. *Kolloid Z. Z. Polym.* **1973**, 251, 980–990.
- (59) Jabbari-Farouji, S.; Lame, O.; Perez, M.; Rottler, J.; Barrat, J.-L. Role of the Intercrystalline Tie Chains Network in the Mechanical Response of Semicrystalline Polymers. *Phys. Rev. Lett.* **2017**, *118*, 217802
- (60) Seguela, R. Critical review of the molecular topology of semicrystalline polymers: The origin and assessment of intercrystalline tie molecules and chain entanglements. *J. Polym. Sci., Part B: Polym. Phys.* **2005**, 43, 1729–1748.
- (61) Huang, Y.-L.; Brown, N. The effect of molecular weight on slow crack growth in linear polyethylene homopolymers. *J. Mater. Sci.* **1988**, 23, 3648–3655.
- (62) Detrez, F.; Cantournet, S.; Seguela, R. Plasticity/damage coupling in semi-crystalline polymers prior to yielding: Micromechanisms and damage law identification. *Polymer* **2011**, *52*, 1998–2008.
- (63) Pawlak, A.; Galeski, A.; Rozanski, A. Cavitation during deformation of semicrystalline polymers. *Prog. Polym. Sci.* **2014**, *39*, 921–958.
- (64) Rozanski, A.; Galeski, A. Plastic yielding of semicrystalline polymers affected by amorphous phase. *Int. J. Plast.* **2013**, *41*, 14–29.
- (65) Jabbari-Farouji, S.; Rottler, J.; Lame, O.; Makke, A.; Perez, M.; Barrat, J.-L. Plastic Deformation Mechanisms of Semicrystalline and Amorphous Polymers. ACS Macro Lett. 2015, 4, 147–150.
- (66) Sarasua, J. R.; Arraiza, A. L. p.; Balerdi, P.; Maiza, I. Crystallinity and mechanical properties of optically pure polylactides and their blends. *Polym. Eng. Sci.* **2005**, *45*, 745–753.
- (67) Bucknall, C. B.; Paul, D. R. Notched impact behaviour of polymer blends: Part 2: Dependence of critical particle size on rubber particle volume fraction. *Polymer* **2013**, *54*, 320–329.
- (68) Bucknall, C. B.; Paul, D. R. Notched impact behavior of polymer blends: Part 1: New model for particle size dependence. *Polymer* **2009**, *50*, 5539–5548.

- (69) Ishai, O.; Coheno, L. J. Effect of Fillers and Voids on Compressive Yield of Epoxy Composites. *J. Compos. Mater.* **1968**, *2*, 302–315.
- (70) Bucknall, C. B.; Davies, P.; Partridge, I. K. Rubber toughening of plastics. *J. Mater. Sci.* **1986**, *21*, 307–313.
- (71) Bucknall, C. B. Rubber toughening. In *The Physics of Glassy Polymers*; Haward, R. N., Young, R. J., Eds.; Springer Netherlands: Dordrecht, 1997; pp 363–412.
- (72) Bucknall, C. B.; Clayton, D.; Keast, W. E. Rubber-toughening of plastics. *J. Mater. Sci.* 1972, 7, 1443–1453.
- (73) Reding, F. P.; Brown, A. Effect of Spherulites on Physical Properties of Fluorothene. *Ind. Eng. Chem.* **1954**, *46*, 1962–1967.
- (74) Huang, Y.-L.; Brown, N. Dependence of slow crack growth in polyethylene on butyl branch density: Morphology and theory. *J. Polym. Sci., Part B: Polym. Phys.* **1991**, 29, 129–137.
- (75) Kramer, E. J. Microscopic and Molecular Fundamentals of Crazing; Springer: Berlin, Heidelberg, 1983; pp 1-56.
- (76) Brown, H. R.; Kramer, E. J. Craze microstructure from small-angle x-ray scattering (SAXS). *J. Macromol. Sci., Part B: Phys.* **1981**, 19, 487–522.
- (77) Kramer, E. J.; Berger, L. L. Fundamental Processes of Craze Growth and Fracture; Springer: Berlin, Heidelberg, 1990; pp 1-68.
- (78) Donald, A. M. Crazing. In *The Physics of Glassy Polymers*, 2 ed.; Haward, R. N., Eds.; Springer Sciences: United Kingdom, 1997; pp 295–341.
- (79) Donald, A. M. Failure Mechanisms in Polymeric Materials. In *Rubber Toughened Engineering Plastics*; Collyer, A. A., Ed.; Springer Sciences: United Kingdom, 1994; pp 1–28. DOI: 10.1007/978-94-011-1260-4 1
- (80) Kramer, E. J. Craze fibril formation and breakdown. *Polym. Eng. Sci.* **1984**, *24*, 761–769.
- (81) Brown, H. R.; Sindoni, Y.; Kramer, E. J.; Mills, P. J. Diffraction studies of craze structure. *Polym. Eng. Sci.* 1984, 24, 825–832.
- (82) Donald, A. M.; Kramer, E. J. Craze microstructure and molecular entanglements in polystyrene-poly(phenylene oxide) blends. *Polymer* **1982**, *23*, 461–465.
- (83) Butler, M. F.; Donald, A. M. A Real-Time Simultaneous Smalland Wide-Angle X-ray Scattering Study of in Situ Polyethylene Deformation at Elevated Temperatures. *Macromolecules* **1998**, *31*, 6234–6249.
- (84) Donald, A. M. X-Ray Scattering Methods in the study of Polymer Deformation. In *Mechanical Properties and Testing of Polymers: An A–Z Reference*; Swallowe, G. M., Ed.; Springer: Netherlands Dordrecht, 1999; pp 278–280. DOI: 10.1007/978-94-015-9231-4 60
- (85) Butler, M. F.; Donald, A. M.; Ryan, A. J. Time resolved simultaneous small- and wide-angle X-ray scattering during polyethylene deformation-II. Cold drawing of linear polyethylene. *Polymer* **1998**, 39, 39–52.
- (86) Gebizlioglu, O. S.; Beckham, H. W.; Argon, A. S.; Cohen, R. E.; Brown, H. R. A new mechanism of toughening glassy polymers. 1. Experimental procedures. *Macromolecules* **1990**, *23*, 3968–3974.
- (87) Argon, A. S.; Cohen, R. E.; Gebizlioglu, O. S.; Brown, H. R.; Kramer, E. J. A new mechanism of toughening glassy polymers. 2. Theoretical approach. *Macromolecules* **1990**, *23*, 3975–3982.
- (88) Brown, H. R.; Argon, A. S.; Cohen, R. E.; Gebizlioglu, O. S.; Kramer, E. J. New mechanism for craze toughening of glassy polymers. *Macromolecules* 1989, 22, 1002–1004.
- (89) Michaels, A. S.; Bixler, H. J. Flow of gases through polyethylene. *J. Polym. Sci.* 1961, 50, 413–439.
- (90) Spiegelberg, S. H.; Argon, A. S.; Cohen, R. E. Kinetics of crazing in polybutadiene/polystyrene blends. *J. Appl. Polym. Sci.* **1994**, 53, 1251–1259.
- (91) Qin, J.; Argon, A. S.; Cohen, R. E. Toughening of glassy polymers by prepackaged deformation-activated diluents. *J. Appl. Polym. Sci.* **1999**, *71*, 1469–1490.
- (92) Mooney, D. J.; Baldwin, D. F.; Suh, N. P.; Vacanti, J. P.; Langer, R. Novel approach to fabricate porous sponges of poly(d,l-lactic-co-

- glycolic acid) without the use of organic solvents. *Biomaterials* **1996**, 17, 1417–1422.
- (93) Bowden, P. B.; Young, R. J. Deformation mechanisms in crystalline polymers. *J. Mater. Sci.* **1974**, *9*, 2034–2051.
- (94) Millot, C.; Séguéla, R.; Lame, O.; Fillot, L.-A.; Rochas, C.; Sotta, P. Tensile Deformation of Bulk Polyamide 6 in the Preyield Strain Range. Micro-Macro Strain Relationships via in Situ SAXS and WAXS. *Macromolecules* **2017**, *50*, 1541–1553.
- (95) Frank, F. C.; Keller, A.; O'Connor, A.; Wills, H. H. Deformation processes in polyethylene interpreted in terms of crystal plasticity. *Philos. Mag.* **1958**, *3*, 64–74.
- (96) Kiho, H.; Peterlin, A.; Geil, P. H. Polymer Deformation. VI. Twinning and Phase Transformation of Polyethylene Single Crystals as a Function of Stretching Direction. *J. Appl. Phys.* **1964**, *35*, 1599–1605
- (97) Wang, D.; Shao, C.; Zhao, B.; Bai, L.; Wang, X.; Yan, T.; Li, J.; Pan, G.; Li, L. Deformation-Induced Phase Transitions of Polyamide 12 at Different Temperatures: An in Situ Wide-Angle X-ray Scattering Study. *Macromolecules* **2010**, *43*, 2406–2412.
- (98) Chen, X.; Lv, F.; Su, F.; Ji, Y.; Meng, L.; Wan, C.; Lin, Y.; Li, X.; Li, L. Deformation mechanism of iPP under uniaxial stretching over a wide temperature range: An in-situ synchrotron radiation SAXS/WAXS study. *Polymer* **2017**, *118*, 12–21.
- (99) Flory, P. J.; Yoon, D. Y. Molecular morphology in semicrystal-line polymers. *Nature* **1978**, *272*, 226–229.
- (100) Zhu, P.; Dong, X.; Wang, D. Strain-Induced Crystallization of Segmented Copolymers: Deviation from the Classic Deformation Mechanism. *Macromolecules* **2017**, *50*, 3911–3921.
- (101) Brüning, K.; Schneider, K.; Roth, S. V.; Heinrich, G. Kinetics of Strain-Induced Crystallization in Natural Rubber Studied by WAXD: Dynamic and Impact Tensile Experiments. *Macromolecules* **2012**, *45*, 7914–7919.
- (102) Xiong, B.; Lame, O.; Chenal, J.-M.; Rochas, C.; Seguela, R.; Vigier, G. Temperature-Microstructure Mapping of the Initiation of the Plastic Deformation Processes in Polyethylene via In Situ WAXS and SAXS. *Macromolecules* **2015**, *48*, 5267–5275.
- (103) Hu, Y.; Rogunova, M.; Topolkaraev, V.; Hiltner, A.; Baer, E. Aging of poly(lactide)/poly(ethylene glycol) blends. Part 1. Poly-(lactide) with low stereoregularity. *Polymer* **2003**, *44*, 5701–5710.
- (104) Ruokolainen, J.; Fredrickson, G. H.; Kramer, E. J.; Ryu, C. Y.; Hahn, S. F.; Magonov, S. N. Effect of Thermal History and Microdomain Orientation on Deformation and Fracture Properties of Poly(cyclohexylethylene)—Polyethylene Triblock Copolymers Containing Cylindrical PE Domains. *Macromolecules* **2002**, 35, 9391—9402.
- (105) Tant, M. R.; Moskala, E. J.; Jank, M. K.; Pecorini, T. J.; Hill, A. J. Craze Initiation and Failure in Glassy Poly(ethylene Terephthalate): The Effects of Physical Aging with and Without Exposure to Chemical Environments. In *Structure and Properties of Glassy Polymers*; American Chemical Society, 1999; Vol. 710; pp 242–257.
- (106) Hill, A. J.; Heater, K. J.; Agrawal, C. M. The effects of physical aging in polycarbonate. *J. Polym. Sci., Part B: Polym. Phys.* **1990**, 28, 387–405.